Deep learning identification of SST teleconnections driving early-winter North Atlantic climate

Víctor Galván Fraile[1,2*], Irene Polo[1†], Marta Martín-Rey[1†], Belén Rodríguez-Fonseca[1,2†], Magdalena A. Balmaseda[3]

[1]Departamento de Física de la Tierra y Astrofísica, Universidad Complutense de Madrid, Madrid, Spain.
[2]Instituto de Geociencias (IGEO), CSIC-UCM, Madrid,Spain.
[3]Research Department, European Centre for Medium Range Weather Forecasts, Reading, United Kingdom.

*Corresponding author(s). E-mail(s): vgalva01@ucm.es;
†These authors contributed equally to this work.

Abstract

Preprint Statement: This manuscript is a non-peer reviewed preprint submitted to EarthArXiv. The preprint was submitted to *npj Climate and Atmospheric Science* for consideration as a research article.

Seasonal predictability over the North Atlantic-European (NAE) sector is strongly modulated by the background climate state, particularly in early winter. In this season, different ENSO teleconnections have been reported before and after the 1990s. However, these studies rely on linear analysis, and the reasons for this lack of stationarity and its implications for seasonal forecasting have not yet been fully assessed. Here, we evaluate the non-stationarity of early winter ENSO teleconnections over the NAE using a non-linear framework, the Neural Network forecast application (NN4CAST). The NN4CAST model predicts November-December sea level pressure anomalies from October sea surface temperature anomalies. The neural network achieves skill comparable to the ECMWF SEAS5 dynamical system, and even exceeds it in certain regions like the NAE, despite relying only on October SST predictors. The model detects a period with significant improvement in skill over the North Atlantic Oscillation centres of action during 1970-1990s, specially for the Iceland region, whereas for the East Atlanticn pattern, the improvement comes in recent decades, namely 1990-2020s. These changes in predictability might be driven by an intensification of the Rossby wave source over Southeast Asia as well as a southward displacement of the North Atlantic jet stream during the latter period. Our results highlight the value of explainable artificial intelligence for identifying state-dependent sources

of seasonal predictability and for bridging data-driven approaches with physical understanding of climate teleconnections.

1 Introduction

Seasonal climate prediction targets the subseasonal to seasonal (S2S) timescale, which corresponds to extended-range weather forecasting (10-30 days) up to the first part of long-range forecasting (from 30 days up to 2 years). In this timescale, atmospheric memory is generally weak, but slowly evolving boundary conditions, may yield predictive skill [1–3]. Forecasting at these lead times, support decision making in multiple sectors, including energy planning, agriculture and risk management [1, 4]. Over the North Atlantic–European (NAE) sector, atmospheric variability is shaped by tropical and extratropical ocean boundary conditions in a seasonally modulated and intermittently predictable manner, especially in boreal winter [5–8].

A key question for the NAE sector concerns early winter (ND, November-December). Relative to late winter (JF, January-February), early-winter teleconnections are less robust, more sensitive to the background state, and less consistently captured by dynamical models [9]. For example, although the North Atlantic Oscillation (NAO) can be internally driven by eddy-mean flow interaction [10], El Niño-Southern Oscillation (ENSO) can also drive it in some decades, with evidence of non-linearity [11–13]. Indeed, studies point out a change in the impact of ENSO in the NAE sector in ND from resembling a NAO pattern in the 1970s and 1980s, to a East Atlantic (EA) in the late 1990s and 2000s [14, 15]. Moreover, Tropical Atlantic and Indian Ocean SST anomalies as well as decadal variability of the Pacific and Atlantic oceans, may further interact to condition the extratropical response [16–18]. Disentangling these overlapping features and identifying whether precursor SST patterns in previous months provide a stable and interpretable source of information for early winter NAE predictions remains an open research challenge.

Despite decades of development in Earth System Models, dynamical seasonal forecast systems exhibit geographically and state-dependent performance, and their skill is often limited by persistent systematic biases [7–9, 19]. In particular, dynamical models frequently underrepresent the strength of observed teleconnections, a manifestation of the signal-to-noise paradox in seasonal prediction, which reduces confidence in simulated teleconnection amplitudes and in operational forecast signals over the NAE [20]. As a consequence, forecast confidence remains episodic and is strongly modulated by background climate conditions and the strength of remote forcings [9, 21, 22]. These limitations motivate complementary strategies that preserve physical insight while exploiting data-driven sources of predictability.

Machine Learning (ML), and in particular Deep Learning (DL), has recently emerged as a promising complement to dynamical and traditional statistical approaches [23]. Classical statistical techniques (e.g., Maximum Covariance Analysis, regression-based predictors) have long been used to diagnose teleconnections and construct empirical predictors [24–26]. Advances in DL provide enhanced capacity to

extract nonlinear relationships, disentangle overlapping modes of variability, and handle spatiotemporal complexity in large datasets [27]. Moreover, explainable AI (XAI) methods offer a pathway to identify physically meaningful precursor structures and increase interpretability beyond black-box predictions [28]. Although some studies have already applied DL to seasonal forecasting, the limited interpretability of these models hinders understanding of the dynamical drivers underlying the learned predictability [29–31]. Additionally, hybrid strategies that pair dynamical model output with ML-based post-processing have also shown promising results in correcting model biases and amplifying predictable signals [32, 33].

In this study, we build a neural network (NN) based model using the NN4CAST framework [34], which has been specifically developed to better understand teleconnections and their associated sources of predictability. Here, we assess the predictive value of tropical and Northern Hemisphere October sea surface temperature (SST) for early-winter mean sea-level pressure (SLP). We evaluate whether this data-driven approach can identify precursor patterns, sources of predictability as well as changes in the teleconnection mechanisms. Specifically, we benchmark the DL forecasts against the operational SEAS5 dynamical prediction system [35]. After verifying that the level of skill obtained is competitive, we then proceed to identify the sources of predictability in NN4CAST. The goals of this work are:

- Quantify the extent to which early-winter SLP anomalies are predictable from previous late-autumn ocean conditions using a DL model.
- Characterise temporal variability of the NAE sector, and assess whether the NN4CAST can capture non-stationary changes in predictability.
- Identify the SST precursor patterns learned by the DL model and interpret their dynamic plausibility and consistency with known physical mechanisms of teleconnection.

The paper is structured as follows: Section 2 presents the results, including benchmarking of skill against SEAS5, identification of dominant predictable modes and time dependence of sources of predictability. Section 3 presents the main conclusions of this study. Finally, Section 4 describes the data and methods of this work.

2 Results

2.1 Evaluation of NN4CAST seasonal prediction skill

We begin by assessing the predictive skill of ND SLP anomalies over the tropics and Northern Hemisphere. To achieve this, we compare two different methodological frameworks: a NN based on the NN4CAST tool and the SEAS5 dynamical seasonal forecast system (see Methods for a description of the framework configurations). For the statistical method, October tropical and Northern Hemisphere SST anomalous fields are used as the predictors, whereas for the dynamical system, the October ensemble mean initialization is used for comparison. It is important to note that NN4CAST follows a deterministic framework and therefore predicts the ensemble mean rather than the full distribution of possible outcomes. This choice is motivated by the objective of

identifying predictable modes of variability, which are expected to be primarily captured by the ensemble mean, as well as by the intention of isolating the main sources of predictability.

Figure 1 summarizes the temporally aggregated performance of these approaches in terms of the anomaly correlation coefficient (ACC) and the root mean square error (RMSE), over the common hindcast period [1981-2019] (see Methods). During the 40-year common assessment period, the pattern of early-winter skill (1-2 month lead time) demonstrated by NN closely resembles that of the dynamical model (Fig. 1a,b). This is a remarkable result considering that the deep learning model takes only information from one specific driver of predictability (SSTs). In comparison with SEAS5, the NN shows similar RMSE levels overall, but with enhanced ACC in specific regions such as the central North Atlantic, the Amazon basin, and parts of the Indian Ocean (Fig. 1c). These results suggest that the NN provides added value in selected regions and metrics. Additionally, comparison with a classical statistical method based on MCA confirms the robustness of the NN results, with comparable or slightly higher ACC and a systematic reduction in RMSE across most regions (Fig. S1 of Supplementary Material). The variability of the predicted signal with respect to the observed one is better captured by the NN model than the SEAS5 ensemble mean, which may be a consequence of the signal-to-noise paradox of dynamical systems [36] (see Fig. S2 of Supplementary Material). Given the competitive performance of NN4CAST over the NAE region against SEAS5, the following section focuses on a detailed regional assessment of the North Atlantic sector.

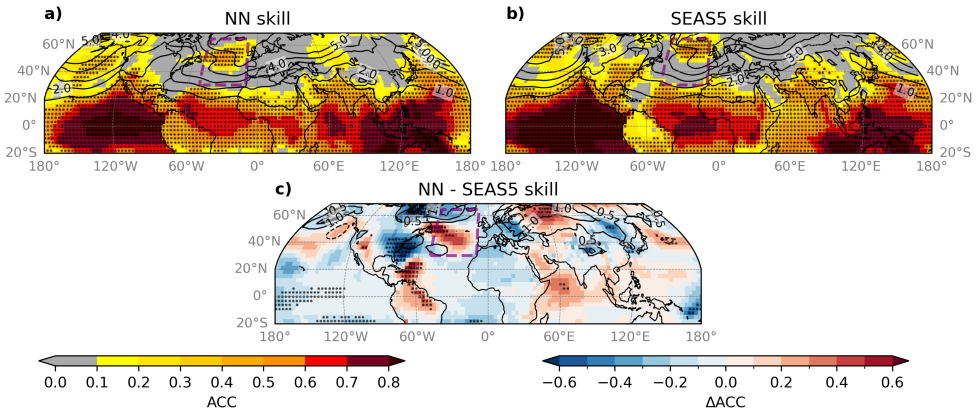

Fig. 1 Skill of seasonal early-winter (ND) predictions from the NN (a) and SEAS5 (b) with a lead time of 2-3 months. Anomaly correlation coefficient and root mean square errors are represented, for the period 1981-2019, in shading and contours, respectively. Differences between models skill are also represented (c). Stippling represents significant skill at the 95% confidence level. The purple rectangle indicate the NAE region [30°N-65°N, 50°W-10°W].

2.2 Predictability of dominant modes of NAE SLP variability

We next focus the analysis on the NAE sector [30°N-65°N, 50°W-10°W], and explore the temporal modulation of early-winter ND SLP skill. To investigate the sources of predictability over the NAE, we analyze the dominant modes of ND SLP variability using an Empirical Orthogonal Functions (EOF) decomposition [37] (Fig. 2). The first two EOFs explain the largest fraction of the total variance in observations (36.9% and 27.3%, respectively) and are, therefore, retained for further analysis. The leading mode of variability corresponds to the NAO, whereas the second mode is associated with the EA pattern (2a-d). The NN successfully reproduces the large-scale structure of both modes, as indicated by the high spatial correlations between observed and predicted patterns (0.94 for EOF_1 and 0.91 for EOF_2).

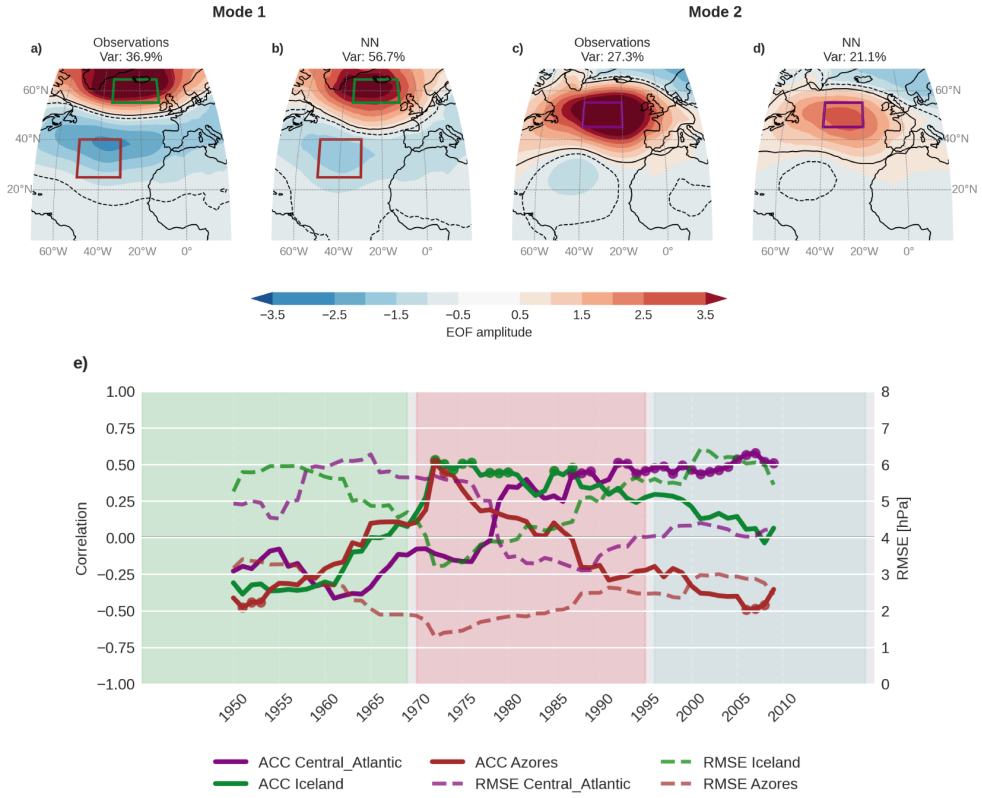

Fig. 2 Predictive skill of early-winter SLP variability in the NAE region. Leading EOF modes of observed (a,c) and predicted (b,d) SLP variability, the explained variance fraction is indicated in each panel. Green, red and purple boxes denote the Iceland, Azores and Central Atlantic regions, respectively. (e) 21-year centred moving correlations (solid lines) and RMSE (dashed lines) between observed and predicted centres of action. Shaded areas in (e) indicate the periods P_0, P_1, and P_2. Contours in EOFs and stippling in moving correlations denote statistical significance at 95% confidence level.

To provide a more physically interpretable framework, we define a set of regional indices based on the centres of action that most strongly capture the amplitude and variability of each mode. For EOF_1 (NAO), we consider the Iceland [55°N-65°N, 35°W-10°W] and Azores [25°N-40°N, 50°W-30°W], while for EOF_2 (EA) we focus on the Central Atlantic [45°N-55°N, 40°W-20°W] (boxes shown in Fig. 2a-d). Using these indices, we compute 21-year centred running correlations and RMSE between observed and predicted SLP anomalies (Fig. 2e), which highlight a pronounced non-stationarity in predictability. In particular, correlations over the Iceland and Azores regions peaks during 1970-1995 (P_1 hereafter), indicating that the NAO related centres of action are more predictable during this period, specially the northern one. In contrast, skill in the Central Atlantic region is maximised during 1996-2019 (P_2), pointing to an enhanced predictability of the EA pattern in this period. During 1940-1969 (P_0), none of the indices present significant skill, which is consistent with findings from coupled simulation experiments [11]. RMSE values for the three indices tend to decrease during decades of higher correlations. SEAS5 exhibits comparable non-stationarity during the common hindcast period, though its skill is displaced northward relative to the NN model (Fig. S3). Due to the limited length of the SEAS5 reforecast, this comparison is restricted to P_2. Since period P_1 and P_2 offer the highest potential for SST-driven statistical prediction, we focus the remainder of our analysis on these two windows. Time series of the indices and skill metrics are provided in the Supplementary Material (Fig. S4 and Tab. S1). Finally, to simplify the subsequent discussion, the Azores index is omitted hereafter due to its limited predictive skill.

2.3 Large-scale teleconnection mechanisms and their modulation of predictability in NAE variability modes

We next examine the physical mechanisms underlying the skilful periods identified for each regional index by analysing their associated teleconnection patterns. To this end, we regress each index onto global anomalous SST, geopotential (Φ_{200}), wave activity flux (WAF) and Rossby wave source (RWS), considering both observed and NN-predicted indices (Fig. 3) (see Methods for variables preprocessing description).

For the Iceland index during P_1, the observed and predicted regressions show a consistent large-scale response characterized by a prominent RWS in the central tropical Pacific, indicative of ENSO forcing (red dots in Fig. 3a,b). This forcing excites a wave train that propagates north-eastward across the Pacific-North American sector and onward into the NAE region, projecting onto a circulation pattern that, in the end, favours a negative NAO-like response over the North Atlantic (coloured contours and green vectors in Fig. 3a,b). Additionally, RWS signals are detected near the entrance of the East Asian jet stream, however, these do not appear to generate an efficient downstream propagation toward the NAE region (blue dots and green arrows in Fig. 3a,b). For the Azores index, similar patterns as for the Iceland index are obtained in P_1, but with a reduced amplitude in the signal due to the lower and less stable predictive skill for this area (see Fig. S5 in the Supplementary Material).

In contrast, the Central Atlantic index displays a different behaviour compared to the Iceland one during its active phase (P_2 in Fig. 3g,h). The SST regressions for this period suggest that, while the central Pacific signal persists, the signal from the eastern

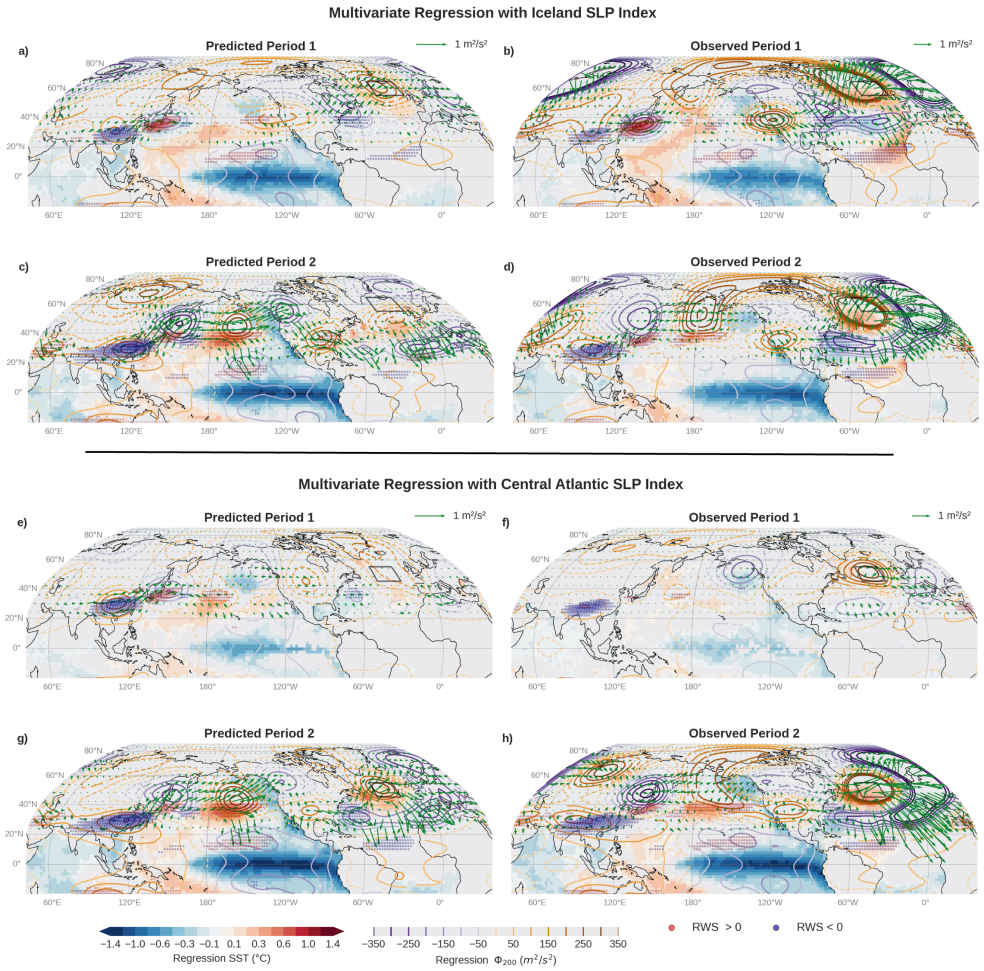

Fig. 3 Teleconnection mechanisms underlying skilful NAE indices. Regression patterns of the Iceland (a-d) and Central Atlantic (e-h) indices onto global anomalous SST (shading), geopotential (Φ_{200}; contours), wave activity flux (WAF; arrows) and Rossby wave source (RWS; stippling) during periods P_1 and P_2. First column panels show regressions using NN-predicted indices, while second column panels show regressions based on observed indices. Only statistically significant SST anomalies are shown, whereas for Φ_{200}, continuous contours denote statistically significant anomalies. The significance level is set to 90% confidence in all panels.

Pacific is intensified. This configuration is accompanied by a strengthened Aleutian Low and an atmospheric circulation response that closely resembles a Pacific-North American pattern. Furthermore, a reinforced SST signal emerges in the extratropical North Pacific. This regional warming might reflect the dynamical coupling with the Aleutian Low by modulating the surface heat fluxes in the area. The impact over the NAE resembles the EA pattern, which is consistent with recent studies pointing to a strengthened relationship between ENSO and the EA since the 1990s [14, 15].

In addition to the Pacific contribution, significant influence from the Indian Ocean is detected, together with a pronounced intensification of the RWS over Mainland Southeast Asia (blue dots in Fig. 3g,h).

The same regression analysis was repeated for the lower skill periods, namely Central Atlantic during P_1 and Iceland during P_2 (see Fig. 3c-f). For the Central Atlantic indices, no clear or coherent SST-forced signal is found, consistent with the reduced skill in this period (Fig. 3e,f). However, for the Iceland index, a wave propagation pattern partially resembling that of the active phase of the Central Atlantic is still observed (Fig. 3c,d). This behaviour can be attributed to the spatial overlap between the Iceland centre of action and the second EOF mode (Fig. 2a-d), which allows part of the associated teleconnection structure to persist even when the primary ENSO forcing is less favourable. It should be noted that teleconnections are not symmetric, and regression analyses assume symmetry and linearity with respect to forcing intensity, which may not fully capture the observed patterns [6, 38, 39].

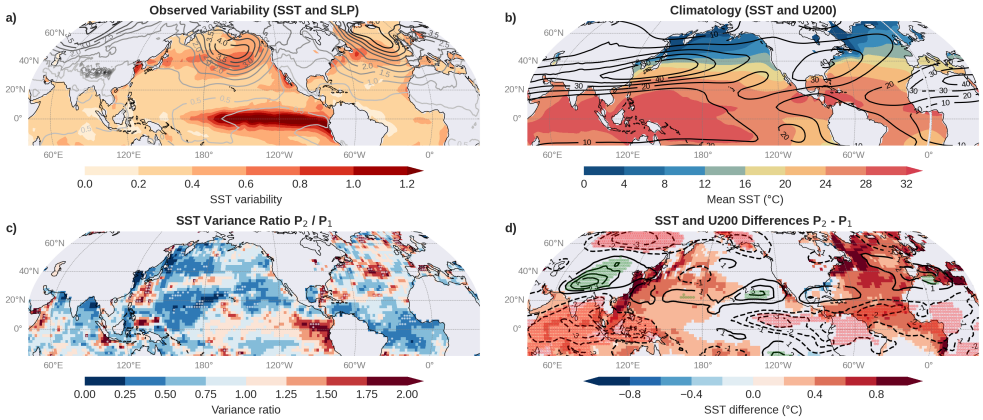

Fig. 4 Changes in early-winter (ND) variability and mean state. Climatology of SLP (contours) and SST (shaded) variability (a), and SST (shaded) and U200 (contours) mean state (b). SST variance ratio between periods P_1 and P_2 (c), where stippling indicates significant changes in variance. Differences in mean state between periods P_1 and P_2 (d) of SST (shaded, only significant) and U200 (contours, red and green for significant negative and positive levels, respectively). The significant level is set to 95% confidence in all subplots.

To diagnose the physical origin of this state dependence, we relate the skill changes to variations in the ocean background conditions of each period, including changes in both SST variability and the mean climate state. Figure 4a highlights the observed October SST and SLP variability, emphasizing the dominant role of the tropical Pacific as a source of variability. The subsequent transition from period P_1 to P_2 [1970-1995 to 1996-2019] is associated with a reduction of SST variability in large parts of the Pacific basin, except for an increase in the eastern equatorial Pacific (Fig. 4c). This result is consistent with a stronger influence of the eastern Pacific in driving the teleconnection during P_2 (Fig. 3e-f). Additionally, an enhanced SST variability is

present during P_2 over the northern part of the Maritime Continent (Fig. 4c), which can be related with the strengthened RWS over this region detected in the regression patterns (Fig. 3g,h). In terms of mean state changes, a warming of the SST in found mainly in the North Atlantic, Indian Ocean as well as Maritime Continent. This SST warming over the Pacific warm pool affects the upper level circulation, leading to an intensification of the East Asian jet stream through the thermal wind balance [40] (Fig. 4d). This intensification may enhance the efficiency of Rossby wave propagation from the East Asian wave source, allowing the wave train to propagate more robustly across the Pacific. Additionally, the southward displacement of the North Atlantic jet stream (black contours in Fig. 4d) likely favours a more equatorward propagation of the Pacific wave train, shifting the region of maximum predictability toward the central North Atlantic.

The changes in SST variability as well as jet stream mean states help to explain the partial degradation and spatial redistribution of Euro-Atlantic skill during recent decades (Fig. 1). Overall, this analysis suggests that the NN skill over the Euro-Atlantic sector is tightly controlled by changes in ENSO variability and low-frequency background SST and U200 states, which may modulate both the strength and the spatial structure of the associated teleconnection pathways [41, 42]. These changes in skill are also present for the MCA and SEAS5 models (see Fig. S3 of the Supplementary Material).

2.4 What drives NN4CAST predictability of NAO and EA variability?

We next investigate how the NN exploits the October SST predictor field to generate skilful forecasts over the NAE sector by applying the Integrated Gradients (IG) attribution method (see Methods). This approach allow us to quantify the relative contribution of each predictor grid point to the predicted indices, thereby providing insights into the internal functioning of the model. The IG analysis is performed separately for the Central Atlantic and Iceland indices, distinguishing between positive and negative phases and across periods P_1 and P_2 (see Methods for composite map calculations). To facilitate physical interpretation, the SST predictor field is partitioned into a set of oceanic regions (Fig. 5a). This partition choice is made according to the ocean basins and the changes in variability from the central and eastern Pacific analysed in Figure4. The IG contributions are spatially aggregated within each region, yielding the regional importance distributions shown in Fig. 5b.

For the negative Iceland index during P_1, the model derives its information primarily from the Pacific basin (accounting up to 80% of the predicted signal), particularly from eastern and central Pacific (light and dark blue boxes), with a secondary contribution from Indian Ocean and extratropical Pacific (orange and dark red boxes) (Fig. 5b). Notice that for the positive Iceland index, the extratropical Pacific forcing becomes more important than the tropical one. The role of the Pacific as the main driver in this period is consistent with the wave propagation pathways identified in the regression analysis (Fig. 3a,b). This influence is reduced during P_2, a period where the model relies more on the eastern tropical Pacific as the dominant source of the predictive signal

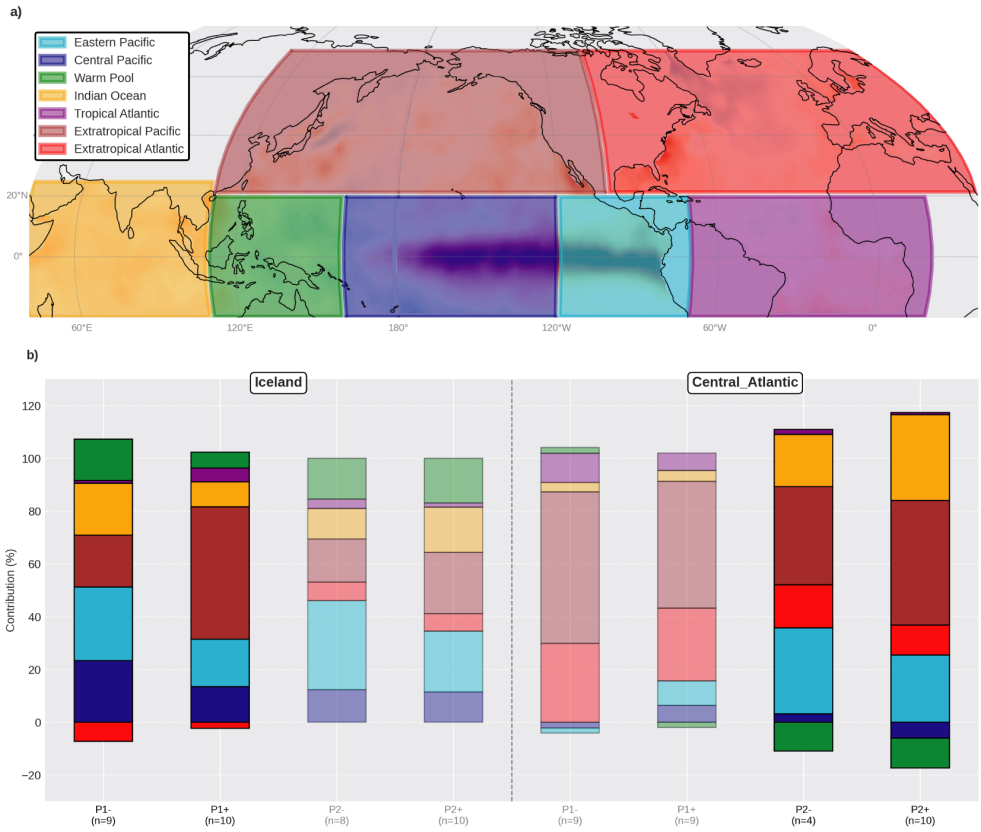

Fig. 5 Regional SST contributions to NN predictions inferred from Integrated Gradients. Partition of the October SST predictor field into oceanic regions used to aggregate Integrated Gradients (IG) contributions (a). Relative contribution (%) of each SST region to the NN predictions of the Iceland and Central Atlantic indices, computed separately for positive and negative phases and for periods P_1 [1970-1995] and P_2 [1996-2019] (b). Periods highlighted correspond to the skilful regimes (P_1 for Iceland; P_2 for Central Atlantic). Contributions represent spatially aggregated IG attributions normalized by the total absolute contribution.

For both signs of the Central Atlantic index during P_2, the predictions are mostly controlled by SST anomalies in the eastern and extratropical Pacific (around 60% of the signal), in agreement with the enhanced SST variability in this region (Fig. 4c). This agrees with a more skilful prediction of the second EOF mode during this period, which resembles the EA pattern. Furthermore, the Indian Ocean emerges as a significant contributor during P_2 for the Central Atlantic index (20% of the signal). This feature is consistent with the intensified RWS over Mainland Southeast Asia identified in Figure 3g-h, suggesting that the NN effectively integrates information from multiple ocean basins when such forcing becomes dynamically relevant. Overall, the IG results demonstrate that the NN adapts its reliance on different SST regions depending on the background climate state, providing a physically interpretable explanation

for the state-dependent predictability analysed in previous sections. These changes in the region of importances are also present for period P_0 and for the Azores region (see Fig. S6 of the Supplementary Material).

These findings motivate a more detailed composite analysis of the key SST patterns associated with the Iceland index in P_1, and the Central Atlantic index in P_2. While the regression analysis provide a linear overview of the teleconnections, the attributions distribution shown in Figure 5 suggest a non-linear behaviour between the positive and negative phases of the indices. Since NN are inherently capable of capturing such non-linearities, we employ composite maps to identify the phase-specific regions and dynamical mechanisms that drive the NAE SLP signal in the model on each period. To this end, years with positive and negative predicted index values are analysed separately. By doing so, the composites incorporate all predicted events, including both well and poorly predicted cases, in order to provide a comprehensive view of model state-dependent behaviour. These composites are constructed from anomalous fields of SST, model importance, observed and predicted SLP, and the associated upper-tropospheric response in terms of Φ_{200}, RWS and WAF (Figs. 6,7).

For positive Iceland index conditions during P_1, the composite analysis reveals a remarkable consistency between observed and predicted SLP patterns, both in terms of spatial structure and magnitude (shaded and black contours in Fig. 6a). This high degree of similarity provides confidence that the model is accurately capturing the key centres of action of the NAO, which define the ENSO impact over the NAE variability during this period [14]. Moving to the second row (contours in Fig. 6b), the SST anomalies for these events coincide with a cooling of the tropical Pacific and the Aleutian sector. Model contributions align with this areas, indicating that they contribute to increase the SLP over the Iceland region for this period (shaded in Fig. 6b). SLP anomalies around the Aleutian sector act as a modulator of vertical wave propagation, which can modulate the Rossby waves propagation emanating from the Pacific and propagating downstream towards the North Atlantic [43] (Fig. 6c). This pathway is shown in Figure 6e, having its source mainly in the central tropical Pacific. For negative Iceland index conditions, the predicted and observed SLP patterns present a stronger positive NAO phase, possibly due to a stronger forcing of those years. The SST anomalies for these events coincide with Niño conditions in the tropical Pacific, which greatly contribute to the predicted negative anomalies over Iceland, and with a reduced importance of the extratropical Pacific compared to the positive events (Fig. 6d). The wave propagation is also intensified, with a stronger RWS over the central Pacific which triggers the wave that propagates towards the NAE (Fig. 6f). Comparison between well predicted events and poorly predicted ones, show that the former are characterised primarily by a well-defined equatorial Pacific forcing, particularly for the positive cases (Figs. S7 and S8 of the Supplementary Material). This suggests that poorly predicted years may be influenced by other forcings beyond SST variability, or by a stronger role of internal atmospheric variability.

For positive Central Atlantic index conditions during P_2, again there is a high consistency between the predicted and observed SLP anomalies (Fig. 7a). The SST pattern associated to this events reveals a eastern Niña pattern, which contributes to enhance the SLP over the Central Atlantic region (Fig. 7c). Additionally, light warm

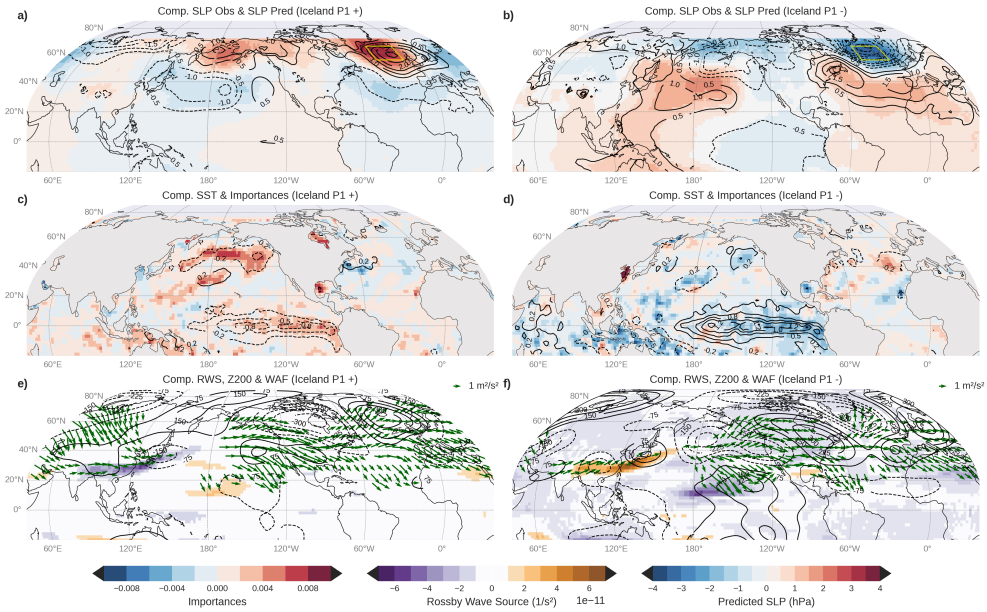

Fig. 6 Composite analysis for the Iceland index during period P_1. Left and right columns represent positive (+) and negative (-) predicted events, respectively. Panels show: (a,b) observed (contours) and predicted (shading) ND SLP anomalies; (c,d) October SST anomalies (contours) and model importances (shaded); and (e,f) ND 200-hPa geopotential anomalies (contours), Rossby wave source (shading), and wave activity flux (vectors). Specific years are for P_1+:[1971,1975,1976,1980,1983,1984,1988,1990,1992,1995] and P_1-:[1972,1977,1982,1986,1987,1991,1993,1994]

anomalies over the southern part of the Maritime Continent appear, contributing positively to the predicted signal over the NAE. The importances pattern is dynamically consistent with a strengthened RWS over the Maritime Continent, as evidenced by the RWS and the subsequent WAF propagation toward the extratropical Pacific and into the Atlantic sector (Fig. 7e). This signal could be related with a stronger role of the Indian Ocean during this period, which has also been assessed in the literature [16, 44]. For the negative events, the SLP pattern presents higher anomalies over the NAE (Fig. 7b), again suggesting a stronger SST forcing for these years. Indeed, the SST composite shows a pattern dominated by an eastern Niño like signal, which also contributes to a large part of the total predicted signal (Fig. 7d). Importances over the Warm Pool might be associated as well with the enhanced RWS over Southeast Asia (Fig. 7d,f). Interestingly, some regions in the subtropical north Atlantic appears as important for the model with opposite-signed contributions (Fig. 7d). These regions may play a complementary role in modulating the strength of the atmospheric response by local air-sea interactions rather than to generate them outright. Furthermore, well-predicted years are associated with a more clearly defined tropical forcing, specially for negative events, which may generate more effective wave propagation toward the NAE sector (see Figs. S9 and S10 of the Supplementary Material).

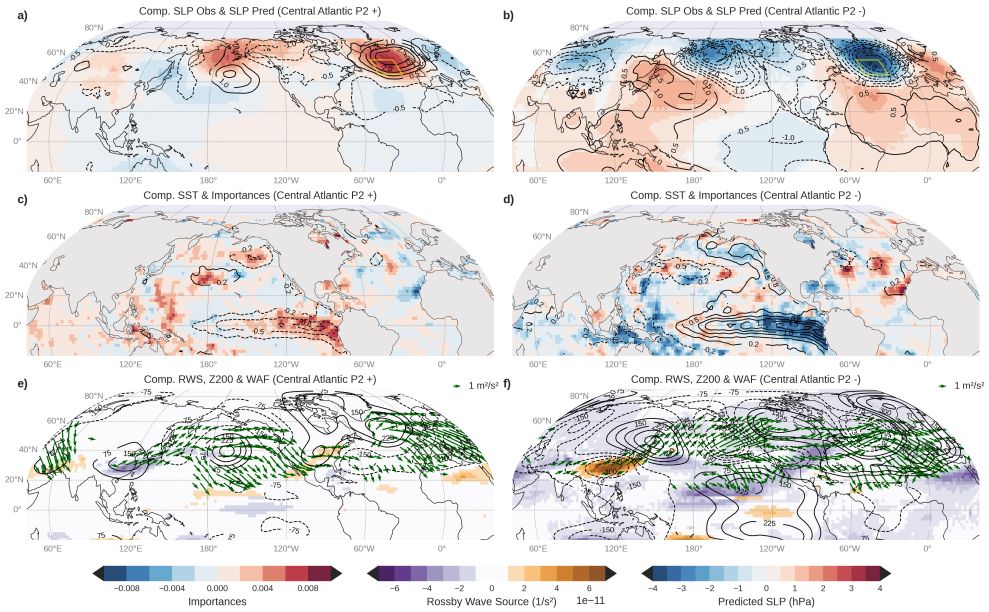

Fig. 7 Same as Fig. 6 but for the Central Atlantic index during period P_2. Specific years are for P_2+:[2001,2003,2005,2007,2010,2011,2016,2019] and P_2-:[1997,2002,2004,2006,2009,2014,2015]

3 Concluding remarks

Using a deep-learning framework (NN4CAST) driven exclusively by October SST anomalies, we demonstrate that neural networks can successfully capture the multi-decadal fluctuations that modulate early-winter seasonal predictability over the NAE sector. Specifically, our framework yields the following findings:

1. Predictive skill over the NAE exhibits decadal shifts that are closely linked to low-frequency changes in tropical SST variability and the large-scale atmospheric and oceanic background circulation.
2. Periods of enhanced NAE predictability coincide with strengthened and spatially coherent ENSO forcing, whereas weaker or spatially displaced tropical variability is associated with reduced or spatially redistributed skill.
3. The neural network successfully reproduces the diversity of ENSO-NAE teleconnection during the observed period, indicates when these patterns are predictable, and provides explanation of the underlying mechanisms:
   (a) Before the mid-1990s (P_1: 1970–1995), ENSO-driven signals primarily project onto a NAO-like pattern, with contributions from tropical and extratropical regions of the Pacific basin.
   (b) After the mid-1990s (P_2: 1996–2019), the teleconnection pathway shifts, becoming more strongly linked to the EA pattern, with additional contribution from the strengthened Rossby wave source over Southeast Asia.

These results highlight the non-stationary nature of seasonal predictability, emphasising that both the strength and the dynamical pathway of the ENSO teleconnections are modulated by the evolving mean state of the coupled system. These regime shifts, linked in recent studies to low-frequency changes such as the Pacific Decadal Oscillation and enhanced Caribbean convection [14, 15], is effectively exploited by NN4CAST, confirming that the model might be capturing physically meaningful precursor signals rather than sampling artefacts.

This capability is particularly noteworthy because coupled dynamical models often struggle to reproduce the full magnitude of these early-winter teleconnections, typically underestimating their amplitude and failing to capture observed multidecadal shifts [9, 15]. In comparison with the SEAS5 dynamical system, NN4CAST achieves a comparable performance in predicting NAE variability. Notably, the neural network reaches this level of skill using exclusively SST information, demonstrating that data-driven approaches can efficiently extract the multi-basin signals that are frequently underrepresented in dynamical frameworks due to the signal-to-noise paradox [11].

A key advance of this work is the application of explainable AI techniques to link predictive skill to identifiable dynamical mechanisms. The NN consistently attributes predictability to SST regions that align with established teleconnection pathways. For example, during periods of high skill of the Central Atlantic, the model attributions combines the informations from the eastward tropical Pacific basin with the Indian Ocean, which agree with previous studies [16]. These attribution patterns are supported by composite and regression analyses, which reveal coherent Rossby wave sources from the central Pacific and Southeast Asia, and downstream wave activity fluxes into the North Atlantic, providing a physically plausible mechanism for the observed skill variability.

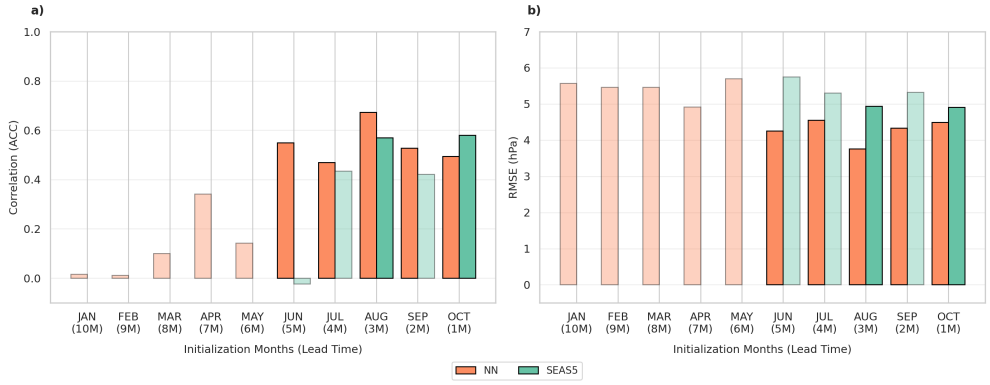

Fig. 8 Lagged skill in terms of ACC (a) and RMSE (b) of Iceland index in the common hindcast of period P_1 [1981-1996]. The horizontal axis represents the months from which the SSTs are taken as the predictor field, and targeting the SLP anomalies in ND. The solid coloured bars represent statistical significant skill with a confidence level of 95

Our results highlight the potential of NN4CAST as a tool for predicting NAE variability and its non-stationary forcings. In this sense, to further explore the temporal horizon of predictability, we extended the analysis by training the NN with SST anomalies from preceding months (e.g., September, August). While skill decreases gradually with increasing lead time, consistent with the reduced persistence of ocean precursors and the growing influence of stochastic atmospheric variability, significant predictive signal remains. Figure 8 summarises this for the Iceland region during P_1 over the common hindcast period between the NN and SEAS5 (1981-1995). It can be seen that, in this period, early-summer SST anomalies may contain useful information for S2S predictability. For the Central Atlantic index during P_2, the skill drops much faster, specially for the NN model (see Fig. S11 on the Supplementary Material).

Overall, these results demonstrate that explainable deep learning offers a powerful complementary framework for seasonal prediction research. By combining competitive forecast skill with mechanistic interpretability, this approach links data-driven inference with process-based understanding of climate variability. Our findings emphasise the potential of regime-aware forecasting strategies that explicitly account for background-state dependence. In practice, this could enhance early-winter predictability over the NAE sector, improving decision-making in sectors such as energy planning, agriculture, and risk management.

4 Methods

4.1 Datasets

We use October mean sea surface temperature (SST) as predictor field, taken from the Met Office Hadley Centre HadISST dataset for the period 1940-2019 [45]. SST fields are considered over the tropical and Northern Hemisphere oceans, spanning the Pacific, Atlantic and Indian Ocean basins (20°S-70°N; 180°W-180°E). The predictand field is early-winter (November-December, ND) mean sea level pressure (SLP) from the ECMWF ERA5 reanalysis, over the same spatial domain and period [46]. To support the physical interpretation of the results, additional atmospheric fields from ERA5 are employed, including geopotential at 200 hPa (Φ_{200}) and zonal and meridional winds at 200 hPa (U200 and V200). These variables are used exclusively for diagnostic analyses and are not included as predictors in the statistical models. To reduce computational cost and ensure consistency across datasets, all variables are regridded to a common $2^\circ \times 2^\circ$ horizontal resolution grid. To filter the lower frequency including long-term trends, a detrending procedure is applied to both predictor and predictand fields using a backward-moving average with a 30-year sliding window. Anomalies are computed over the full dataset period (1940-2019). However, for comparison with SEAS5 they are adjusted to match the reforecast period climatology (1981–2019).

4.2 Models

4.2.1 Neural Network Model

We implement a six-layer artificial neural network using the NN4CAST Python library, which provides a unified framework for data preprocessing, model construction and

training [34]. Model version V1.0.20 is used for this study [47]. The NN is designed to predict early-winter (November-December, ND) SLP anomalies from October SST anomalies, both spanning from the tropics and Northern Hemisphere. The network follows an encoder-decoder architecture. The encoder progressively compresses the high-dimensional SST anomaly field into a low-dimensional latent representation, while the decoder maps this latent space back to the full SLP anomaly field. This configuration allows the model to extract large-scale, physically relevant SST patterns while retaining sufficient flexibility to reconstruct spatially complex atmospheric responses. Model configuration details, including preprocessing choices, architectural parameters and training settings, are summarized in Table 1. The selected architecture is intentionally simple. This choice is motivated by several considerations. First, the limited length of the historical record restricts the effective sample size available for training; a relatively shallow and regularized network reduces the risk of overfitting and improves training stability. Second, a simpler architecture facilitates model interpretability and attribution analyses, enabling a physically meaningful assessment of which SST regions contribute to predictability, beyond maximising forecast skill alone. To make efficient use of the available data and to ensure a robust out-of-sample evaluation, we adopt a leave-one-out (LOO) cross-validation strategy [48]. In each iteration, a single year is held as an independent test sample, while the remaining years are used for training. Skill and attribution diagnostics are then aggregated across all test samples. All predictor and predictand fields are standardized at each grid point using statistics computed from the training years within each cross-validation fold. In addition, multiple realizations of the NN model are generated by varying the random initialization seed, which controls the initialization of the model parameters. Specifically, ensemble-mean results based on 15 different seeds are retained, as this configuration yields improved performance in terms of both ACC and RMSE (see Fig. S12 in the Supplementary Material).

4.2.2 Dynamical seasonal forecast system (SEAS5)

As a dynamical reference, we use the ECMWF SEAS5 seasonal forecasting system [35]. In this study, we focus on the forecasts initialized on October 1st to predict ND SLP anomalies over the common evaluation period. We explicitly avoid the November 1st initialization, as predictions at this shorter lead time are heavily governed by atmospheric initial conditions. This atmospheric memory dominates the early forecast evolution, obscuring the lower-boundary forced signals driven by SSTs. Given that our neural network predicts ND SLP anomalies based only on mean October SSTs, comparing it against the SEAS5 October initialization provides a more equitable assessment of SST-driven predictability. This approach focuses in the evaluation of the forced atmospheric response in both models, despite the minor methodological difference between an instantaneous October 1st initialization and a monthly-averaged October input. For SEAS5, ensemble-mean forecasts are considered, and anomalies are computed relative to the model climatology. Unlike statistical approaches, SEAS5 explicitly represents coupled ocean-atmosphere dynamics, providing a robust, independent benchmark for assessing the added value of the data-driven methods.

Hyperparameter	Value	Hyperparameter	Value
Input/Output, Temporal and Spatial Settings			
region_predictor	North-Tropical Oceans	time_lims	1940-2019
lat_lims_x	70, -20	lon_lims_x	-180, 180
lat_lims_y	70, -20	lon_lims_y	-180, 180
Preprocessing			
detrend_x/y	True/True	detrend_x/y_window	30/30
mean_seasonal_method_x/y	True/True	regrid_degree_x/y	2/2
months_x	10	months_y	11,12
Model Architecture			
layer_sizes	1024, 256, 64, 256, 1024	activations	ELU
num_conv_layers	0	dropout_rates	0.1
use_dropout	True	use_batch_norm	True
use_initializer	True	kernel_regularizer	l2
Training Settings			
learning_rate	0.0001	epochs	2500
p_value	0.1	jump_year	0
cross_validation	True	CV strategy	Leave-One-Out

Table 1 Table summarizing the selected model hyperparameters and preprocessing settings used in the simulation of Oct SST - ND SLP.

4.3 Indices and Metrics

To characterize regional SLP variability over the NAE sector, we define three standardized SLP indices based on the dominant centres of action identified from the EOF analysis. These indices represent area-averaged ND SLP anomalies over the following regions: Iceland (55°N-65°N, 35°W-10°W) and Azores (25°N-40°N, 50°W-30°W), associated with the leading EOF mode, and Central Atlantic (45°N-55°N, 40°W-20°W), associated with the second EOF mode. For each region, ND SLP anomalies are spatially averaged and standardized using the full-period mean and standard deviation. To assess predictability at interannual time scales and to remove low-frequency variability, a Butterworth high-pass filter is applied to each index. The filter is designed with a cutoff period of 10 years, thereby isolating high-frequency fluctuations while suppressing decadal and longer-term variability. All analyses of skill and teleconnection strength based on the indices are performed using the filtered time series. For the composite analyses, years are classified according to the sign and magnitude of the standardized indices. Years with index values exceeding +0.5 standard deviations are defined as positive events, while years with index values below -0.5 standard deviations are classified as negative events. This threshold ensures a sufficient number of events while retaining a clear separation between opposite phases.

The statistical significance of all the analysis was estimated by means of a bootstrap resampling with 1000 permutations [37].

Model performance is evaluated using two complementary metrics: the Anomaly Correlation Coefficient (ACC) and the Root Mean Square Error (RMSE) [37]. The ACC measures the temporal association between predicted and observed anomalies

and is defined as

$$\mathrm{ACC} = \frac{\sum_{t=1}^{N}(x_t - \bar{x})(y_t - \bar{y})}{\sqrt{\sum_{t=1}^{N}(x_t - \bar{x})^2}\sqrt{\sum_{t=1}^{N}(y_t - \bar{y})^2}}, \tag{1}$$

where x_t and y_t denote the predicted and observed anomalies at time t, respectively, $\bar{x}$ and $\bar{y}$ are their climatologies, and N the number of samples. The RMSE quantifies the magnitude of the prediction error and is defined as

$$\mathrm{RMSE} = \sqrt{\frac{1}{N}\sum_{t=1}^{N}(x_t - y_t)^2}. \tag{2}$$

Together, ACC and RMSE provide complementary information on forecast quality, capturing both the temporal coherence and the amplitude accuracy of the predicted anomalies.

4.4 Wave Diagnostics

The propagation of quasi-stationary Rossby waves is quantified using the Wave Activity Flux (WAF) formulation of Takaya and Nakamura [49], which diagnoses the direction and magnitude of wave energy propagation independently of wave phase and aligned with the local group velocity under the geostrophic approximation. This makes WAF particularly suitable for identifying teleconnection pathways in the upper troposphere. The zonal and meridional components of the WAF at pressure level P are given by

$$\mathrm{WAF}_x = \frac{p\cos\phi}{2|\mathbf{U}|}\left[\frac{u}{a^2\cos^2\phi}\left(\left(\frac{\partial\psi'}{\partial x}\right)^2 - \psi'\frac{\partial^2\psi'}{\partial x^2}\right) + \frac{v}{a^2\cos\phi}\left(\frac{\partial\psi'}{\partial x}\frac{\partial\psi'}{\partial y} - \psi'\frac{\partial^2\psi'}{\partial x\partial y}\right)\right] \tag{3}$$

$$\mathrm{WAF}_y = \frac{p\cos\phi}{2|\mathbf{U}|}\left[\frac{u}{a^2\cos\phi}\left(\frac{\partial\psi'}{\partial x}\frac{\partial\psi'}{\partial y} - \psi'\frac{\partial^2\psi'}{\partial x\partial y}\right) + \frac{v}{a^2}\left(\left(\frac{\partial\psi'}{\partial y}\right)^2 - \psi'\frac{\partial^2\psi'}{\partial y^2}\right)\right] \tag{4}$$

where ϕ is latitude, a is the Earth radius, and $U = (u, v)$ denotes the climatological horizontal wind vector with magnitude $|U|$. The quantity ψ' is the anomalous geostrophic streamfunction, defined as

$$\psi' = \Phi'/f, \tag{5}$$

with Φ' the anomalous geopotential and f the Coriolis parameter. Partial derivatives ∂x and ∂y are taken along the zonal and meridional directions, respectively. In this study, WAF is computed at the 200 hPa level, where upper-tropospheric Rossby wave propagation is typically strongest [50].

To identify the regions where Rossby waves are generated, we analyse the Rossby Wave Source (RWS) formulation, which represents the production of anomalous vorticity by divergent flow in the upper troposphere. In the tropics, this mechanism is closely linked to deep convection and large-scale diabatic heating [51]. The RWS is defined as the advection of the climatological absolute vorticity by the anomalous divergent wind:

$$\mathrm{RWS} = -\mathbf{v}'_\chi \cdot \nabla(\zeta + f), \tag{6}$$

where v'_χ denotes the anomalous irrotational (divergent) wind, ζ is the climatological relative vorticity, and f is the planetary vorticity. This term captures the dominant contribution to upper-tropospheric vorticity forcing in the tropics and is therefore particularly suitable for diagnosing tropical-extratropical teleconnections [52].

4.5 Model Explainability

Model interpretability is assessed using the Integrated Gradients (IG) attribution method, as implemented in the NN4CAST framework, and following the methodology of [34, 53]. IG quantifies the contribution of each input feature to a given model output by integrating the gradients of the model along a straight-line path between a predefined baseline and the actual input. In this study, the baseline is defined as the climatological SST state, represented by a zero-anomaly field. After model training, a single October SST anomaly field is passed through the NN to produce a spatially resolved ND SLP anomaly prediction. For each output grid point k, the IG attribution with respect to an input SST grid point i is computed as

$$\mathrm{IG}_i^{(k)}(x) = (x_i - x_i^{\mathrm{base}}) \int_0^1 \frac{\partial F_k\left(x^{\mathrm{base}} + \alpha(x - x^{\mathrm{base}})\right)}{\partial x_i}\, d\alpha, \tag{7}$$

where F_k denotes the model output at grid point k, x is the input SST anomaly field, and x^{base} is the baseline input. Because the NN predicts a full spatial field rather than a single scalar, the IG computation is performed independently for each output grid point, yielding a distinct SST attribution map for each predicted SLP location and sample. Attribution maps are then aggregated across all leave-one-out cross-validation folds to obtain an estimate of the SST regions that consistently contribute to the prediction of the NAE SLP.

Supplementary information.

Data availability

The gridded reanalysis and observational datasets used in this study are publicly available on their corresponding websites: ERA5, HadISST and SEAS5.

Code availability

The scripts used in this study are available upon request to the corresponding author.

Acknowledgements

This research has been supported by the Spanish Ministry of Science, Innovation and Universities through the National Program FPU (grant no. AP-2022-02162), the Oceans for Future project funded by the European Union Next GenerationEU/PRTR Strategic Projects (grant no. TED2021-130106B-I00 f) and the UCM FEI-EU-25-02. MMR has been supported by Ramón y Cajal (RYC2022-038454-I, funded by MCIN/AEI/10.13039/501100011033 and co-funded by the FSE+, European Union).

Author Contributions

V.G. performed the statistical seasonal predictions, carried out the analysis of the model predictability and wrote the original draft of the manuscript. I.P., M.M., B.R. and M.A. contributed to the supervision, conceptualisation and methodology of the work. All authors reviewed the manuscript.

Competing Interests

The authors declare no competing interests.

References

[1] Hoskins, B.: The potential for skill across the range of the seamless weather-climate prediction problem: a stimulus for our science. Quarterly Journal of the Royal Meteorological Society **139**(672), 573–584 (2013)

[2] Doblas-Reyes, F.J., García-Serrano, J., Lienert, F., Biescas, A.P., Rodrigues, L.R.: Seasonal climate predictability and forecasting: status and prospects. Wiley Interdisciplinary Reviews: Climate Change **4**(4), 245–268 (2013)

[3] Mariotti, A., Baggett, C., Barnes, E.A., Becker, E., Butler, A., Collins, D.C., Dirmeyer, P.A., Ferranti, L., Johnson, N.C., Jones, J., *et al.*: Windows of opportunity for skillful forecasts subseasonal to seasonal and beyond. Bulletin of the American Meteorological Society **101**(5), 608–625 (2020)

[4] Viel, C., Beaulant, A.-L., Soubeyroux, J.-M., Céron, J.-P.: How seasonal forecast could help a decision maker: an example of climate service for water resource management. Advances in Science and Research **13**, 51–55 (2016)

[5] Rodríguez-Fonseca, B., Suárez-Moreno, R., Ayarzagüena, B., López-Parages, J., Gómara, I., Villamayor, J., Mohino, E., Losada, T., Castaño-Tierno, A.: A review of enso influence on the north atlantic. a non-stationary signal. Atmosphere **7**(7), 87 (2016)

[6] Ayarzagüena, B., Ineson, S., Dunstone, N., Baldwin, M., Scaife, A.A.: Intraseasonal effects of el niño–southern oscillation on north atlantic climate. Journal of Climate (2018) https://doi.org/10.1175/jcli-d-18-0097.1

[7] Domeisen, D., Butler, A., Fröhlich, K., Bittner, M., Müller, W., Baehr, J.: Seasonal predictability over europe arising from el niño and stratospheric variability in the mpi-esm seasonal prediction system. Journal of Climate **28**, 256–271 (2015) https://doi.org/10.1175/jcli-d-14-00207.1

[8] Fabiano, F., Christensen, H., Strommen, K., Athanasiadis, P., Baker, A.J., Schiemann, R., Corti, S.: Euro-atlantic weather regimes in the primavera coupled climate simulations: impact of resolution and mean state biases on model performance. Climate Dynamics **54**, 5031–5048 (2020) https://doi.org/10.1007/s00382-020-05271-w

[9] Molteni, F., Brookshaw, A.: Early- and late-winter enso teleconnections to the euro-atlantic region in state-of-the-art seasonal forecasting systems. Climate Dynamics **61**, 2673–2692 (2023) https://doi.org/10.1007/s00382-023-06698-7

[10] Hurrell, J.W., Kushnir, Y., Ottersen, G., Visbeck, M.: An overview of the north atlantic oscillation. Geophysical monograph-American geophysical union **134**, 1–36 (2003)

[11] Weisheimer, A., Schaller, N., O'Reilly, C., MacLeod, D.A., Palmer, T.: Atmospheric seasonal forecasts of the twentieth century: multi-decadal variability in predictive skill of the winter north atlantic oscillation (nao) and their potential value for extreme event attribution. Quarterly Journal of the Royal Meteorological Society **143**(703), 917–926 (2017)

[12] King, M.P., Keenlyside, N., Li, C.: Enso teleconnections in terms of non-nao and nao atmospheric variability. Climate Dynamics **61**(5), 2717–2733 (2023)

[13] Mezzina, B., García-Serrano, J., Bladé, I., Kucharski, F.: Dynamics of the enso teleconnection and nao variability in the north atlantic–european late winter. Journal of Climate **33**(3), 907–923 (2020)

[14] Hou, J., Fang, Z., Geng, X.: Recent strengthening of the enso influence on the early winter east atlantic pattern. Atmosphere **14**(12), 1809 (2023)

[15] Fernández-Castillo, P., Losada, T., Rodríguez-Fonseca, B., García-Maroto, D., Mohino, E., Durán, L.: Multidecadal variability of the enso early-winter teleconnection to europe and implications for seasonal forecasting. npj Climate and Atmospheric Science **8**(1), 272 (2025)

[16] Abid, M.A., Kucharski, F., Molteni, F., Kang, I.-S., Tompkins, A.M., Almazroui, M.: Separating the indian and pacific ocean impacts on the euro-atlantic response to enso and its transition from early to late winter. Journal of Climate **34**(4), 1531–1548 (2021)

[17] Senan, R., Balmaseda, M.A., Molteni, F., Stockdale, T.N., Weisheimer, A., Johnson, S., Roberts, C.D.: The relative role of indian and pacific tropical heating

as seasonal predictability drivers for the north atlantic oscillation. Journal of Geophysical Research: Atmospheres **129**(18), 2024–041233 (2024)

[18] López-Parages, J., Rodríguez-Fonseca, B., Terray, L.: A mechanism for the multi-decadal modulation of enso teleconnection with europe. Climate Dynamics **45**(3), 867–880 (2015)

[19] Sabatani, D., Gualdi, S.: Enso teleconnections with the nae sector during december in cmip5/cmip6 models: impacts of the atmospheric mean state. npj Climate and Atmospheric Science **8**(1), 226 (2025)

[20] Scaife, A.A., Smith, D.M.: A signal-to-noise paradox in climate science. npj Climate and Atmospheric Science **1**, 1–8 (2018) https://doi.org/10.1038/s41612-018-0038-4

[21] Baker, L.H., Shaffrey, L.C., Johnson, S.J., Weisheimer, A.: Understanding the intermittency of the wintertime north atlantic oscillation and east atlantic pattern seasonal forecast skill in the copernicus c3s multi-model ensemble. Geophysical Research Letters **51**(15), 2024–108472 (2024)

[22] O'Reilly, C.: Signal-to-noise errors in early winter euro-atlantic predictions linked to weak enso teleconnections and pervasive jet biases. Quarterly Journal of the Royal Meteorological Society **151** (2025) https://doi.org/10.1002/qj.4952

[23] Burgh-Day, C.O., Leeuwenburg, T.: Machine learning for numerical weather and climate modelling: a review. Geoscientific Model Development **16**(22), 6433–6477 (2023)

[24] Fletcher, C.G., Saunders, M.A.: Winter north atlantic oscillation hindcast skill: 1900–2001. Journal of Climate **19**(22), 5762–5776 (2006)

[25] Wilks, D.S.: Comparison of probabilistic statistical forecast and trend adjustment methods for north american seasonal temperatures. Journal of Applied Meteorology and Climatology **53**(4), 935–949 (2014)

[26] Hall, R.J., Scaife, A.A., Hanna, E., Jones, J.M., Erdélyi, R.: Simple statistical probabilistic forecasts of the winter nao. Weather and Forecasting **32**(4), 1585–1601 (2017)

[27] Reichstein, M., Camps-Valls, G., Stevens, B., Jung, M., Denzler, J., Carvalhais, N., Prabhat, F.: Deep learning and process understanding for data-driven earth system science. Nature **566**(7743), 195–204 (2019)

[28] Guidotti, R., Monreale, A., Ruggieri, S., Turini, F., Giannotti, F., Pedreschi, D.: A survey of methods for explaining black box models. ACM computing surveys (CSUR) **51**(5), 1–42 (2018)

[29] Watt-Meyer, O., Henn, B., McGibbon, J., Clark, S.K., Kwa, A., Perkins, W.A., Wu, E., Harris, L., Bretherton, C.S.: Ace2: accurately learning subseasonal to decadal atmospheric variability and forced responses. npj Climate and Atmospheric Science **8**(1), 205 (2025)

[30] Kent, C., Scaife, A.A., Dunstone, N.J., Smith, D., Hardiman, S.C., Dunstan, T., Watt-Meyer, O.: Skilful global seasonal predictions from a machine learning weather model trained on reanalysis data. npj Climate and Atmospheric Science **8**(1), 314 (2025)

[31] Pinheiro, E., Ouarda, T.B.: An interpretable machine learning model for seasonal precipitation forecasting. Communications Earth & Environment **6**(1), 222 (2025)

[32] Mouatadid, S., Orenstein, P., Flaspohler, G., Cohen, J., Oprescu, M., Fraenkel, E., Mackey, L.: Adaptive bias correction for improved subseasonal forecasting. Nature Communications **14**(1), 3482 (2023)

[33] Avila-Velasquez, D.I., Macian-Sorribes, H., Pulido-Velazquez, M.: Fuzzy postprocessing of seasonal climate forecasts for semiarid river basins. Quarterly Journal of the Royal Meteorological Society, 70050 (2025)

[34] Galván Fraile, V., Rodríguez-Fonseca, M.B., Polo, I., Martín-Rey, M., Moreno-García, M.N.: Assessing seasonal climate predictability using a deep learning application: Nn4cast. EGUsphere **2025**, 1–28 (2025)

[35] Johnson, S.J., Stockdale, T.N., Ferranti, L., Balmaseda, M.A., Molteni, F., Magnusson, L., Tietsche, S., Decremer, D., Weisheimer, A., Balsamo, G., *et al.*: Seas5: the new ecmwf seasonal forecast system. Geoscientific Model Development **12**(3), 1087–1117 (2019)

[36] Scaife, A.A., Smith, D.: A signal-to-noise paradox in climate science. npj Climate and Atmospheric Science **1**(1), 28 (2018)

[37] Wilks, D.S.: Statistical Methods in the Atmospheric Sciences vol. 100. Academic press, ??? (2011)

[38] Zhang, W., Wang, Z., Stuecker, M.F., Turner, A.G., Jin, F.-F., Geng, X.: Impact of enso longitudinal position on teleconnections to the nao. Climate Dynamics **52**(1), 257–274 (2019)

[39] Trascasa-Castro, P., Maycock, A.C., Scott Yiu, Y.Y., Fletcher, J.K.: On the linearity of the stratospheric and euro-atlantic sector response to enso. Journal of Climate **32**(19), 6607–6626 (2019)

[40] Wallace, J.M., Hobbs, P.V.: Atmospheric Science: an Introductory Survey vol. 92. Elsevier, ??? (2006)

[41] López-Parages, J., Rodríguez-Fonseca, B., Dommenget, D., Frauen, C.: Enso influence on the north atlantic european climate: A non-linear and non-stationary approach. Climate Dynamics **47**(7), 2071–2084 (2016)

[42] Branstator, G.: Circumglobal teleconnections, the jet stream waveguide, and the north atlantic oscillation. Journal of Climate **15**(14), 1893–1910 (2002)

[43] Dickinson, R.E.: Planetary rossby waves propagating vertically through weak westerly wind wave guides. Journal of Atmospheric Sciences **25**(6), 984–1002 (1968)

[44] Raganato, A., Abid, M.A., Kucharski, F.: The combined link of the indian ocean dipole and enso with the north atlantic–european circulation during early boreal winter in reanalysis and the ecmwf seas5 hindcast. Journal of Climate **38**(2), 445–460 (2025)

[45] Titchner, H.A., Rayner, N.A.: The met office hadley centre sea ice and sea surface temperature data set, version 2: 1. sea ice concentrations. Journal of Geophysical Research: Atmospheres **119**(6), 2864–2889 (2014)

[46] Hersbach, H., Bell, B., Berrisford, P., Hirahara, S., Horányi, A., Muñoz-Sabater, J., Nicolas, J., Peubey, C., Radu, R., Schepers, D., *et al.*: The era5 global reanalysis. Quarterly journal of the royal meteorological society **146**(730), 1999–2049 (2020)

[47] Galván Fraile, V., Martín-Rey, M., Rodríguez-Fonseca, B., Polo, I., Navarro-García, M.: NN4CASTv1. 0.20, Zenodo [code] (2024)

[48] Géron, A.: Hands-on Machine Learning with Scikit-Learn, Keras, and TensorFlow. " O'Reilly Media, Inc.", ??? (2022)

[49] Takaya, K., Nakamura, H.: A formulation of a wave-activity flux for stationary rossby waves on a zonally varying basic flow. Geophysical research letters **24**(23), 2985–2988 (1997)

[50] Wirth, V., Riemer, M., Chang, E.K., Martius, O.: Rossby wave packets on the midlatitude waveguide—a review. Monthly Weather Review **146**(7), 1965–2001 (2018)

[51] Qin, J., Robinson, W.A.: On the rossby wave source and the steady linear response to tropical forcing. Journal of Atmospheric Sciences **50**(12), 1819–1823 (1993)

[52] Sardeshmukh, P.D., Hoskins, B.J.: The generation of global rotational flow by steady idealized tropical divergence. Journal of Atmospheric Sciences **45**(7), 1228–1251 (1988)

[53] Sundararajan, M., Taly, A., Yan, Q.: Axiomatic attribution for deep networks.

In: International Conference on Machine Learning, pp. 3319–3328 (2017). PMLR

Supplementary information for Deep Learning identification of SST teleconnections driving early-winter North Atlantic Climate

Víctor Galván Fraile [1,2*], Irene Polo [1], Marta Martín-Rey [1], Belén Rodríguez-Fonseca [1,2*], Magdalena A. Balmaseda [3]

[1] Departamento de Física de la Tierra y Astrofísica, Universidad Complutense de Madrid, Madrid, Spain.

[2] Instituto de Geociencias (IGEO), CSIC-UCM, Madrid, Spain.

[3] Research Department, European Centre for Medium Range Weather Forecasts, Reading, United Kingdom.

S1 Supplementary Material

1.1 Maximum Covariance Analysis Model

As a linear statistical benchmark, we apply Maximum Covariance Analysis (MCA) to relate October SST anomalies to ND SLP anomalies (Durán et al. , 2024). MCA identifies pairs of spatial patterns in the predictor and predictand fields that maximize their temporal covariance, providing an optimal linear mapping between the two fields. Only SST information is used as the predictor field, ensuring a fair comparison with the NN. The MCA model is trained and evaluated over the same period and using the same cross-validation framework as the NN, which in this case is a leave-one-out cross-validation.

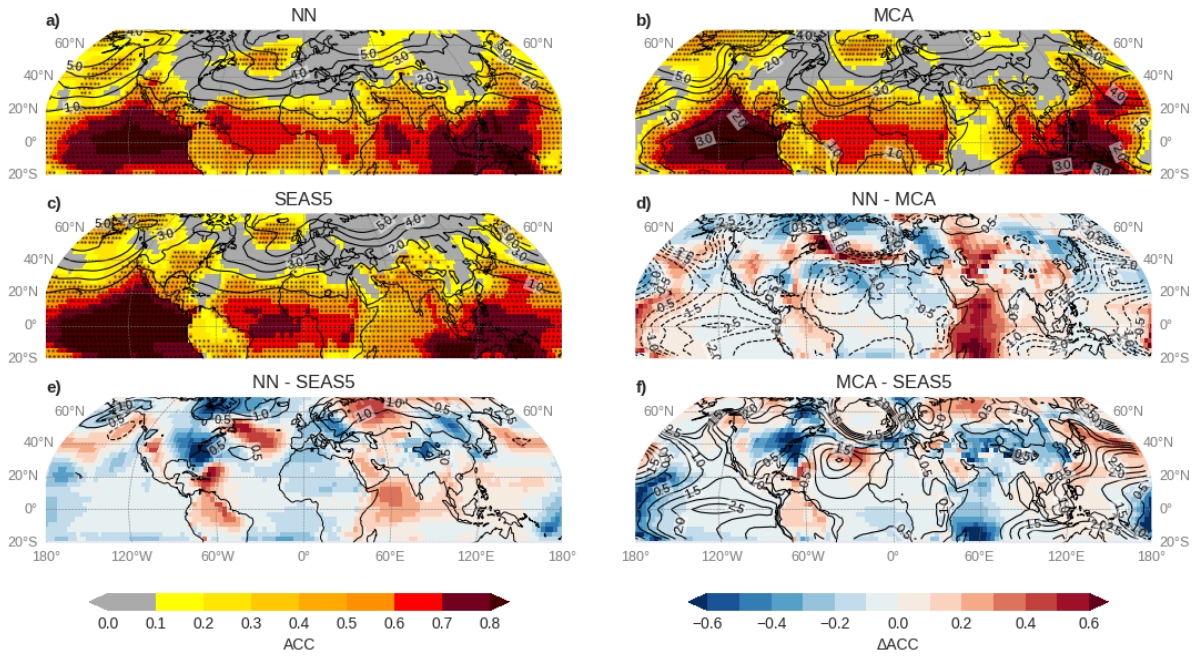

Figure S1: Skill of seasonal early-winter (ND) predictions from the NN (a), MCA (b) and SEAS5 (c) with a lead time of 2-3 months. Anomaly correlation coefficient and root mean square errors are represented, for the period 1981-2016, in shading and contours, respectively. Differences between model skills are also represented (e-f). Stippling represents significant skill at the 95% confidence level.

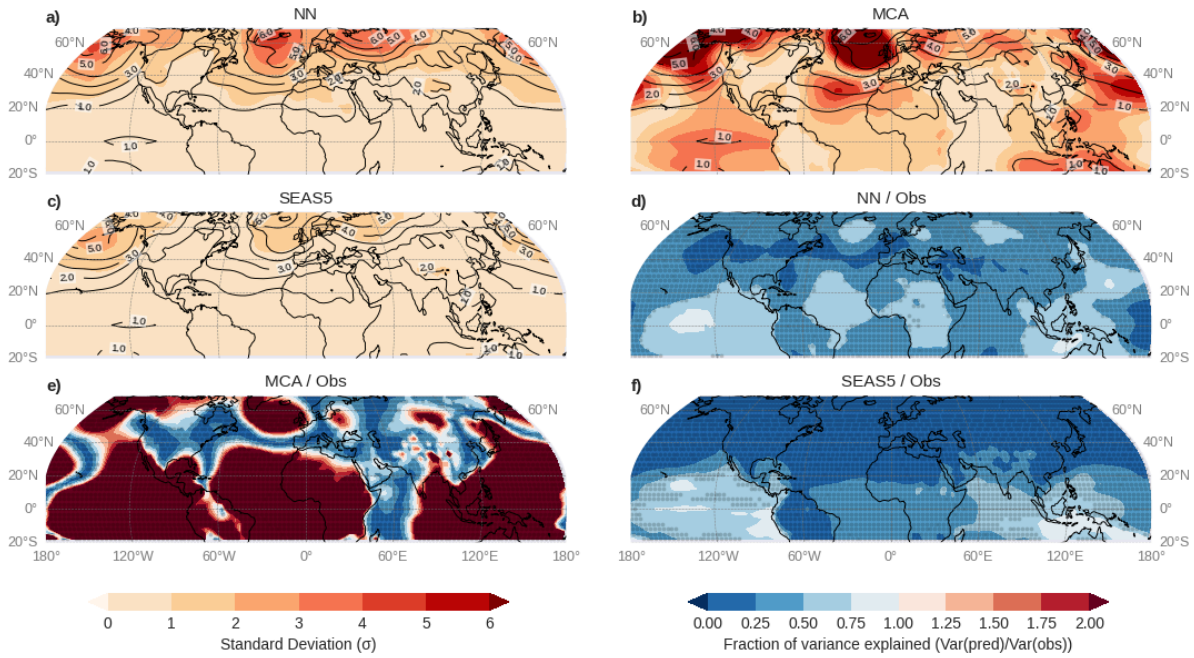

Figure S2: Temporal variability of seasonal early-winter (ND) predictions from the NN (a), MCA (b) and SEAS5 (c) with a lead time of 2-3 months. Predicted and observed standard deviations are represented, for the period 1981-2016, in shading and

colours, respectively. Fractions of variance between predictions and observations are also represented (e-f). Stippling represented significant changes in variance at the 95% confidence level.

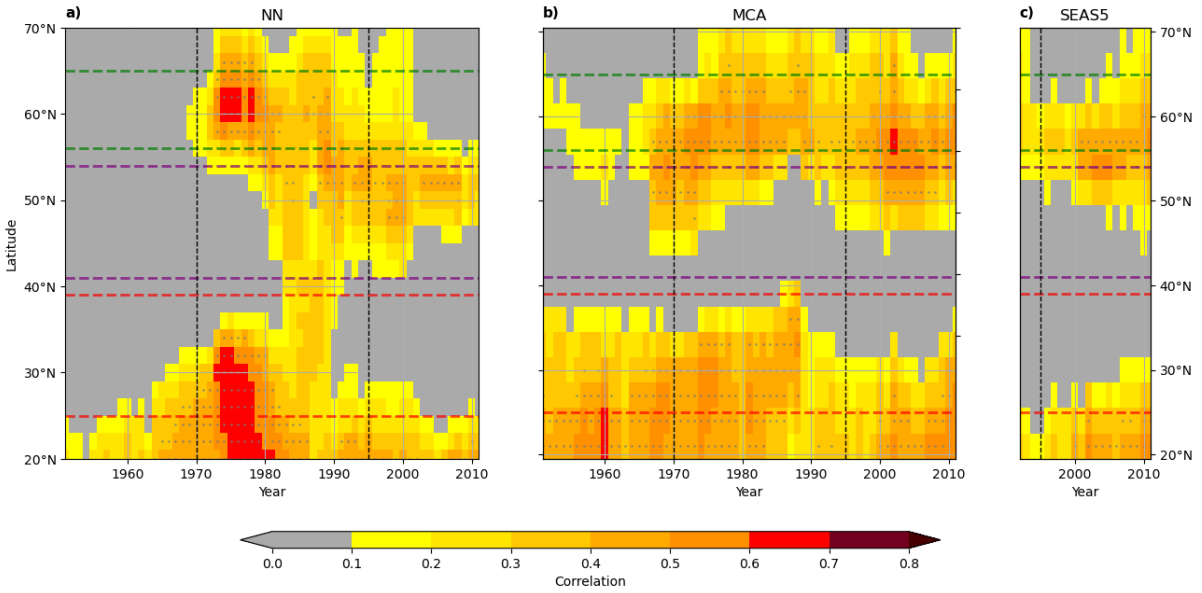

Figure S3: Hovmöller diagram of longitudinal-average seasonal early-winter North Atlantic ACC skill evolution with respect to time for the NN (a), MCA (b) and SEAS5 (c) models with a lead time of 2-3 months. Red, green and blue horizontal lines represent the regions for the Iceland, Central Atlantic and Azores indices, respectively. Stippling indicates significant skill at the 95% confidence level.

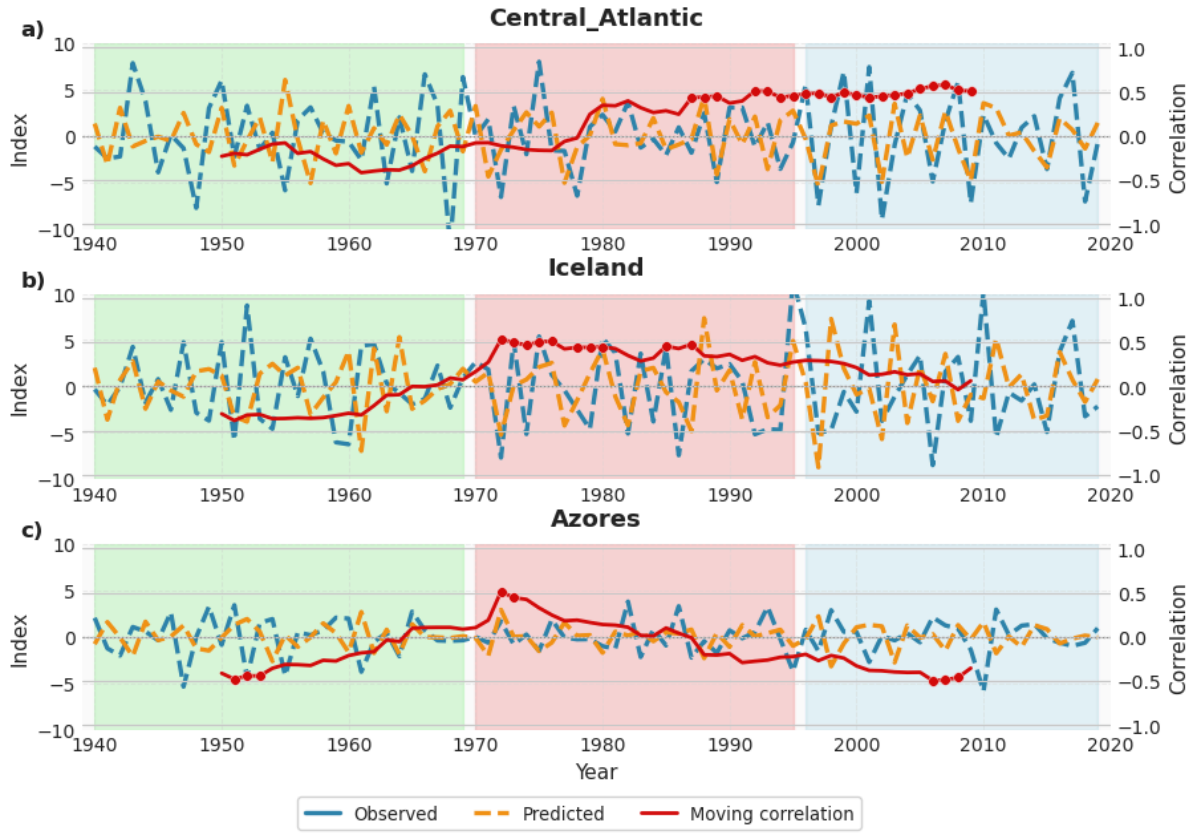

Figure S4: Time series and moving correlations for the Central Atlantic, Iceland and Azores indices for the full hindcast period. Stippling in moving correlations indicates significance at 95% confidence level. Shaded areas indicate the periods: P_0 [1940-1969], P_1 [1970-1995] and P_2 [1996-2019]

Index	*Period*	*ACC*	*RMSE [hPa]*
Central Atlantic	*Full period*	*0.15*	*4.63*
	P_0	*-0.28*	*5.64*
	P_1	*0.22*	*3.63*
	P_2	***0.55***	*4.16*

Iceland	*Full period*	*0.13*	*5.04*
	P_0	*-0.23*	*5.07*
	P_1	***0.49***	*4.14*
	P_2	*0.07*	*5.82*
Azores	*Full period*	*-0.23*	*2.56*
	P_0	*-0.32*	*2.93*
	P_1	*0.20*	*1.86*
	P_2	*-0.48*	*2.71*

Table S1: Summary of model skill metrics for the Central Atlantic, Iceland and Azores indices for the different periods over the hindcast. ACC values in bold indicate statistical significance at 95% confidence level.

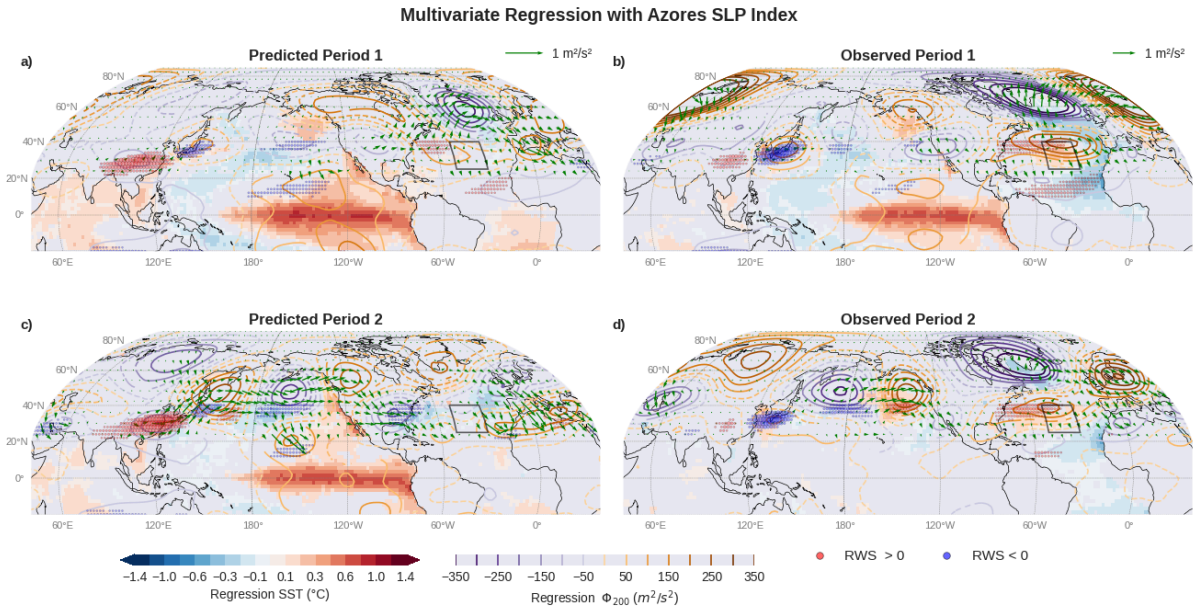

Figure S5: Same as Fig.3 but for the Azores index.

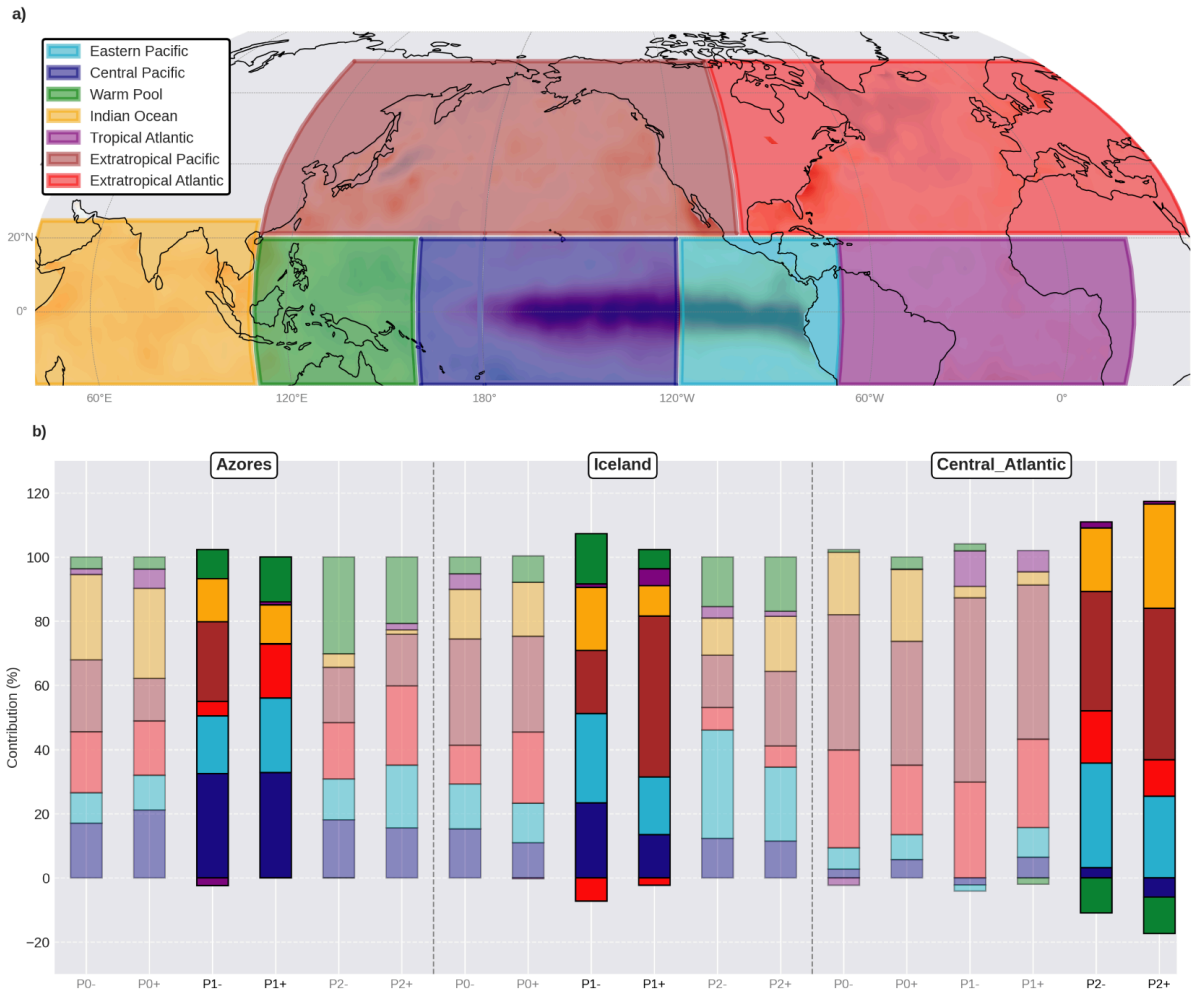

Figure S6: Same as Fig.5 but for the three indices (Azores, Iceland and Central Atlantic) over the periods: P_0 [1940-1969], P_1 [1970-1995] and P_2 [1996-2019].

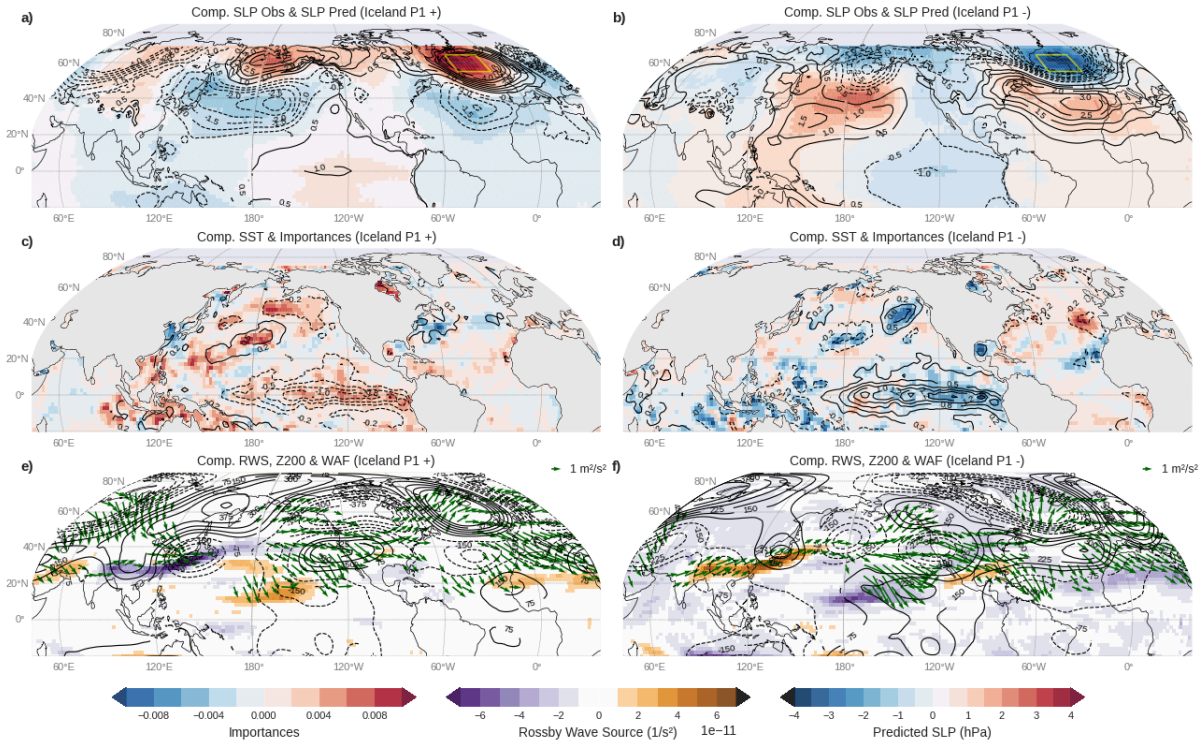

Figure S7: Same as Fig.6 but only for Iceland index in P_1 well predicted events, which correspond to P_1+: [1975,1980,1983,1988,1990,1995] and P_1-: [1972,1982,1986,1993,1994].

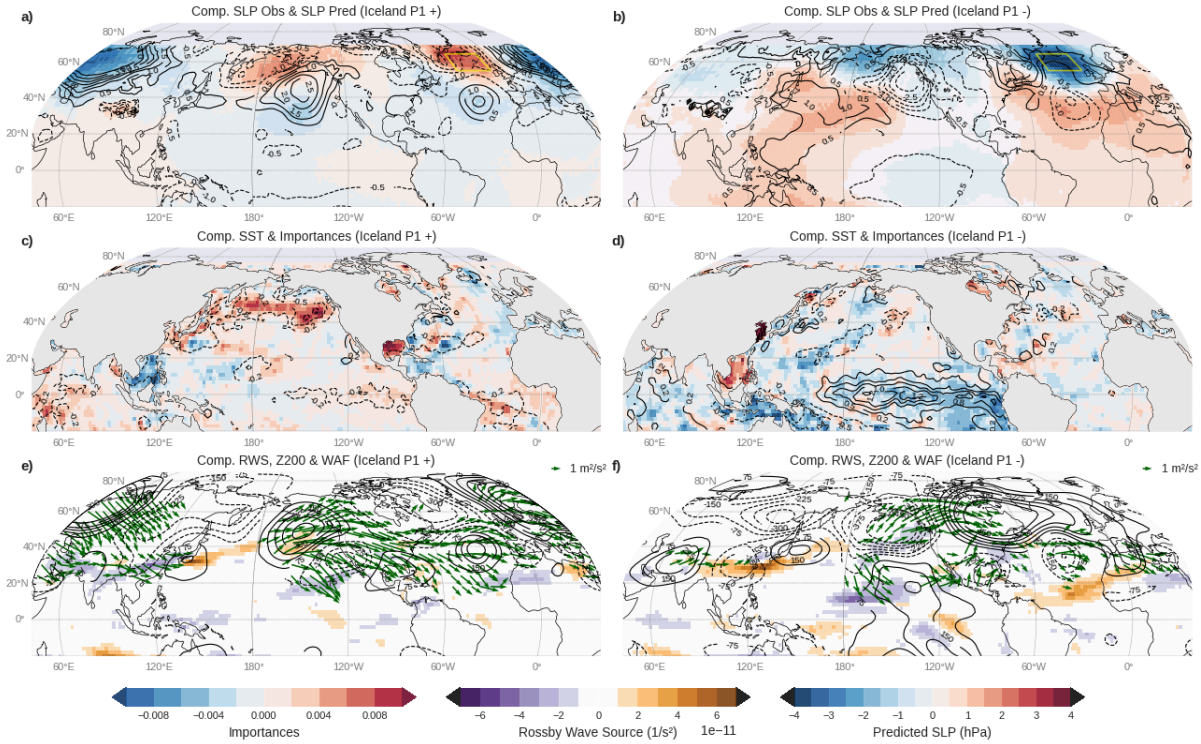

Figure S8: Same as Fig.6 but only for Iceland index in P1 bad predicted events,which correspond to P_1+: [1971,1976,1984,1992] and P_1-: [1977,1987,1991].

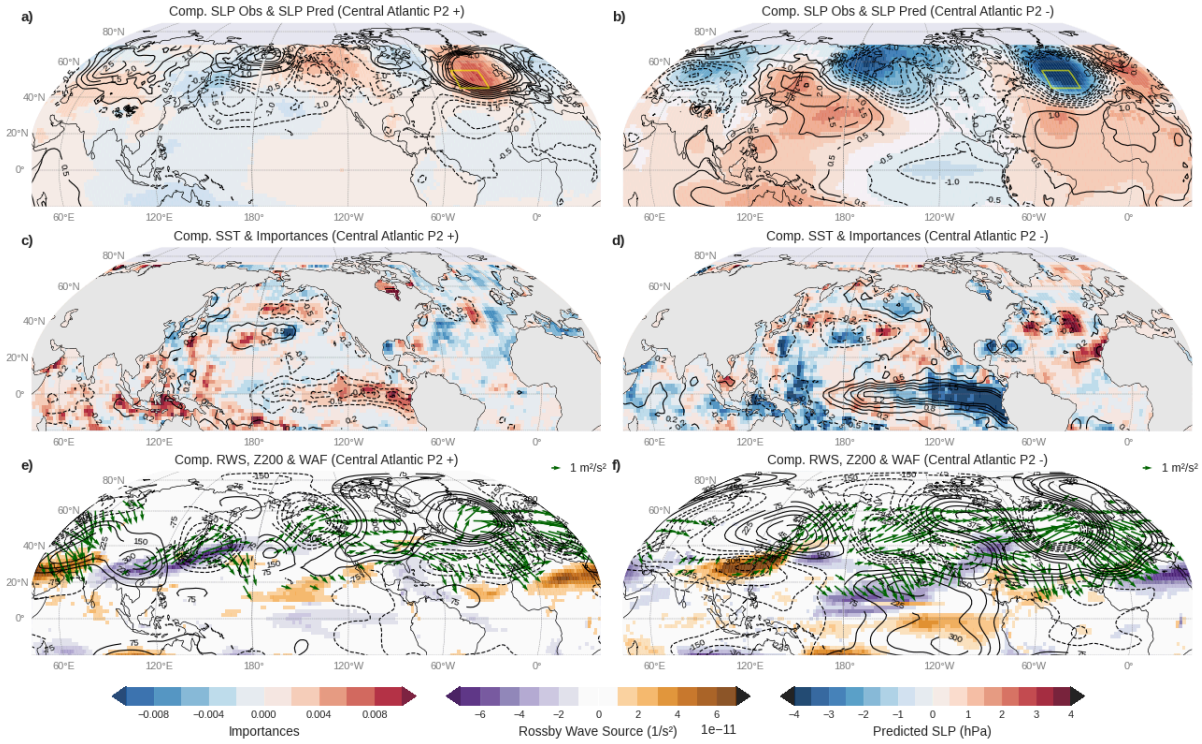

Figure S9: Same as Fig.7 but only for Central Atlantic index in P2 well predicted events, which correspond to P_2+: [2001,2005,2016] and P_2-: [1997,2002,2006,2009,2015].

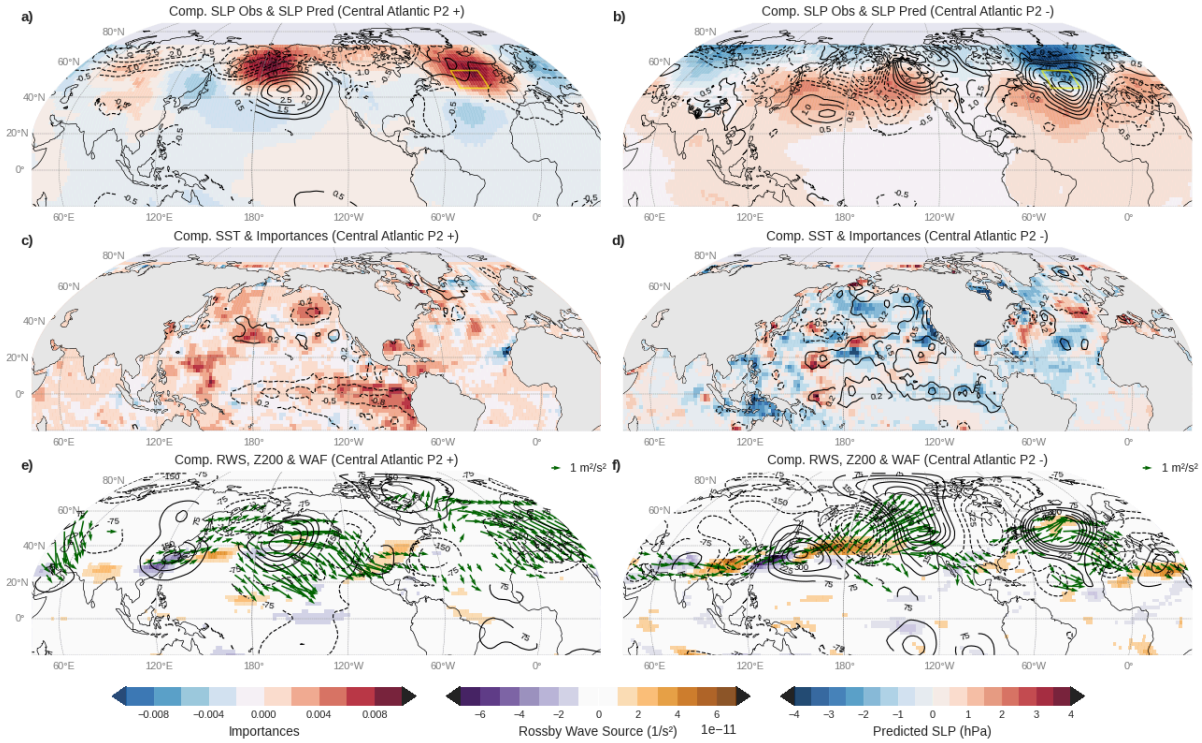

Figure S10: Same as Fig.7 but only for Central Atlantic index in P2 bad predicted events, which correspond to P_2+: [2003,2007,2010,2011,2018] and P_2-: [2004,2014].

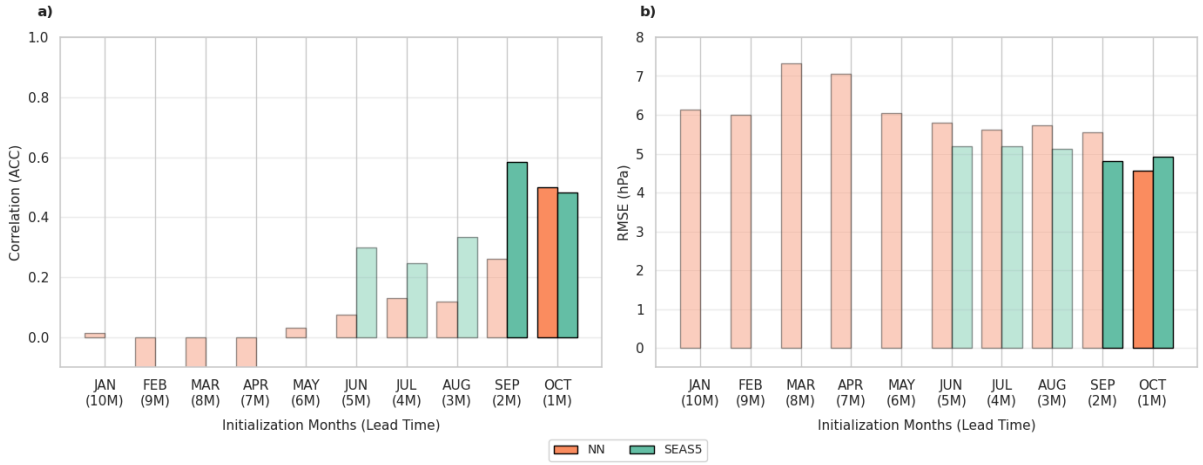

Figure S11: Lagged skill in terms of ACC (a) and RMSE (b) of Central Atlantic in period P2 [1996-2019]. The horizontal axis represents the months from which the SSTs are taken as the predictor field, and targeting the SLP anomalies in ND. The solid coloured bars represent statistical significant skill with a confidence level of 95%.

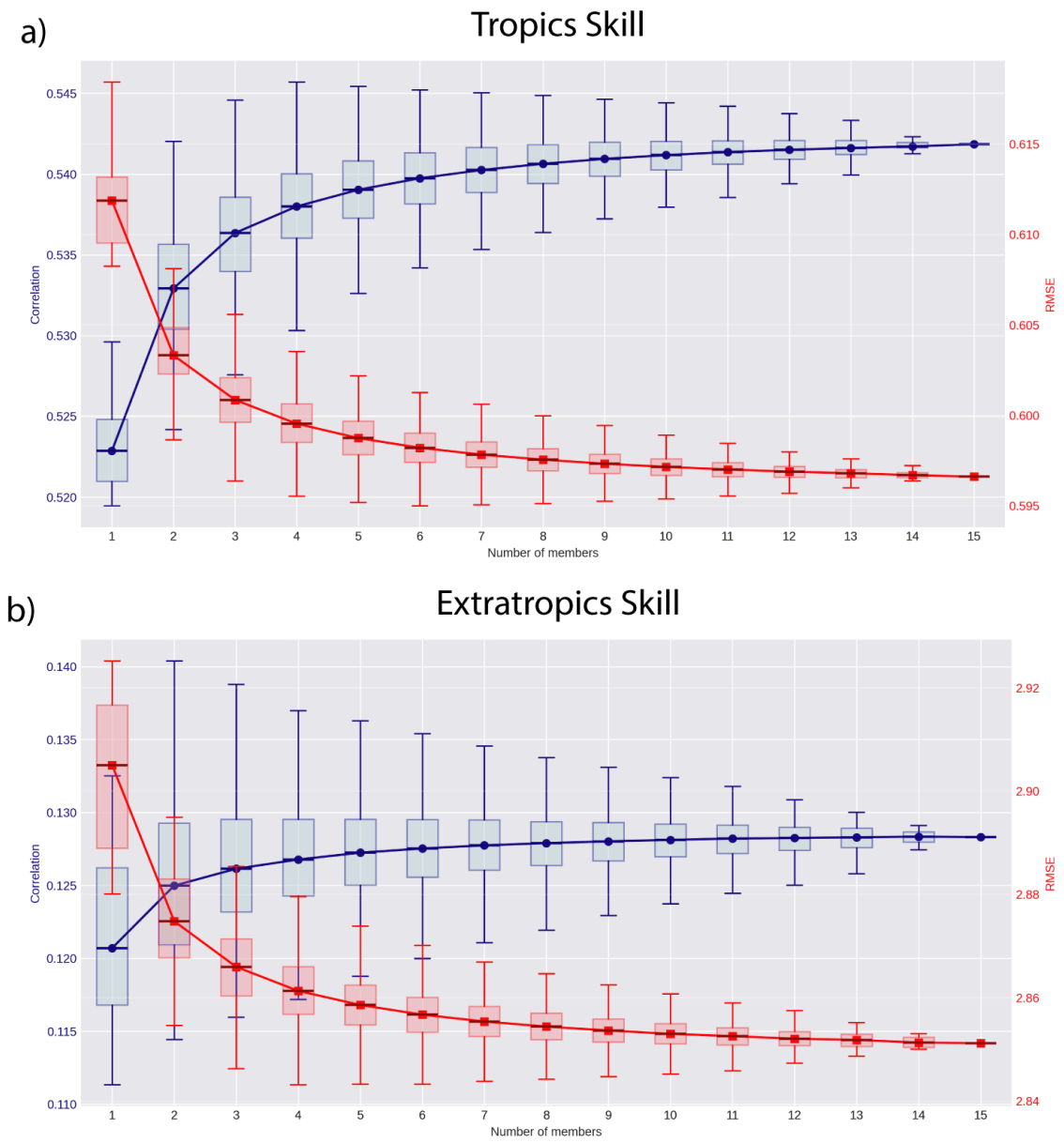

Figure S12: ND model skill in predicting MSLP anomalies over the tropics [20°S-20°N, (a)] and extratropics [20°N-70°N, (b)] as a function of the number of members selected for the period 1940-2019. Y-axes represent on the left the anomaly correlation coefficient between ensemble mean predictions and observations, whereas on the right the same but for the root mean square error.